ESTIMATING FIRE RADIATIVE POWER OBSCURATION BY TREE CANOPIES THROUGH LABORATORY EXPERIMENTS: ESTIMATING FIRE RADIATIVE ENERGY IN A LONGLEAF PINE FOREST FROM AIRBORNE THERMAL IMAGERY

A Thesis

Presented in Partial Fulfillment of the Requirements for the

Degree of Master of Science

with a

Major in Natural Resources

in the

College of Graduate Studies

University of Idaho

by

William Mathews

Major Professor: Eva K. Strand, Ph.D.

Committee Members: Alistair Smith, Ph.D.; Andy Hudak, Ph.D.; Matthew Dickinson, Ph.D.

Department Administrator: Anthony Davis, Ph.D.

July 2015

AUTHORIZATION TO SUBMIT THESIS

This Thesis of William Mathews, submitted for the degree of Master of Science with a Major in Natural Resources and titled "Estimating Fire Radiative Power Obscuration by Tree Canopies Through Laboratory Experiments: Estimating Fire Radiative Energy in a Longleaf Pine Forest from Airborne Thermal Imagery," has been reviewed in final form. Permission, as indicated by the signatures and dates below, is now granted to submit final copies to the College of Graduate Studies for approval.

Major Professor: _____ Date: _____
Eva K. Strand, Ph.D.

Committee Members: _____ Date: _____
Alistair M. S. Smith, Ph.D.

_____ Date: _____
Andy T. Hudak, Ph.D.

_____ Date: _____
Matthew B. Dickinson, Ph.D.

Department Administrator: _____ Date: _____
Anthony S. Davis, Ph.D.

ABSTRACT

The radiant energy released during biomass burning can be measured remotely, and is directly related to the biomass consumed during the fire. One source of error associated with estimating fire radiative energy (FRE) remotely is the obscuration of the signal by the forest canopy. We quantify the relationship between canopy cover and the amount of radiant power observed by a sensor from laboratory experiments. A linear decrease in FRP as a result of simulated canopy cover increase was observed and attenuation of up to 70% was recorded at closed canopy. We applied the canopy correction to thermal imagery collected over a longleaf pine forest in northwestern Florida. Pre-fire LiDAR imagery quantified the forest canopy and surface fuels. From thermal imagery and LiDAR data we predicted the amount of biomass consumed within 6% of field measured fuel consumption from the Florida prescribed burn under a forest canopy.

ACKNOWLEDGEMENTS

I would like say thank you to my major professor Eva Strand who guided and encouraged me through this process. Thank you for your commitment to me and this project especially in these last few weeks, where you willing worked around the clock to help finish this manuscript. I would also like to thank my committee members; Alistair Smith, Andy Hudak, and Matt Dickinson for their guidance and input, which produced a much better product than I could have imagined. Bob Kremens thank you for pulling together all the equipment necessary for making the lab experiment a reality, and of course your colorful outlook on life, the lab would not have been as interesting as it was without you. I would also like to thanks all the faculty that had a hand in making this a better project.

I would also like to thank everyone at the I-FIRE lab that made this research possible. Thank you Kara Yedinak and Alistair Smith for putting your experiments on hold so we could use the fire lab. I would also like to thank Chris Schachtschneider and Kevin Satterberg for sacrificing their weekends to help finish the laboratory section of this project. Also thanks to everyone in Phinney 301-302 offices for letting me make my project our project.

TABLE OF CONTENTS

LIST OF TABLES

LIST OF FIGURES

CHAPTER 1: ESTIMATING FIRE RADIATIVE POWER OBSCURATION BY TREE CANOPIES THROUGH LABORATORY EXPERIMENTS

Abstract

Estimates of biomass burning in wildfires or prescribed fires are needed to account for the production of trace gases and aerosols that enter the atmosphere during combustion. Research has demonstrated that the consumption of biomass is linearly related to fire radiative energy (FRE) released during the burn. FRE estimates are known to be biased by certain environmental characteristics, such as topography and tree canopy cover. Laboratory experiments were conducted to assess the influence of canopy cover on the sensor observed radiant energy. A range of canopy measurements 0 to 90% along with two classes of canopy, non-transpiring living and desiccated branches, were used in the construction of the canopy. Attenuation of energy by the canopy was shown to bias estimates by as much as 70% under a completely closed canopy. Results from this research will contribute to reducing the error in estimates of biomass consumption in surface fires burning under a forest canopy.

Introduction

Fire is a key earth-system process (Bowman *et al.* 2009). Fire impacts the global carbon (C) cycle from both anthropogenic and natural sources, with 1350 – 3400 Tg C emitted from land use changes, agricultural practices, and residential uses; and 2750 – 4600 Tg C emitted in wildfire events that exhibit high inter-annual variability (Westerling *et al.* 2006; Wotton *et al.* 2010; Balch *et al.* 2013) (van der Werf *et al.* 2010). Biomass burning has many direct and indirect effects on the environment, one of which is the production of trace gases and aerosols (Crutzen and Andreae 1990). These emissions directly impact atmospheric

chemistry and have negative social impacts reducing visibility and creating potential health concerns through poor air quality (Andreae and Merlet 2001; Ichoku and Kaufman 2005). Deposition of nitrogen from biomass burning stimulates nitrogen limited ecosystems, increasing growth rates and C accumulation through increased production (Vitousek *et al.* 1997). Understanding emissions from biomass burning is therefore important in characterizing the terrestrial-atmospheric C cycle, and many ecological and social impacts, both positive and negative (Bowman *et al.* 2009).

Traditional methods for estimating biomass burning emissions required extensive knowledge of pre-fire fuels, the degree of combustion completeness, and specific emission factors to quantify gases and particulates produced (Seiler and Crutzen, 1980). Exploration from laboratory experiments of specific chemical compounds and particulates emission factors have produced extensive emission rate coefficients under different combustion phases (Hardy et al. 2001; Yokelson *et al.* 2013). However, difficulty remains in the characterization of pre-fire fuel loading and the factors inherent within combustion completeness (i.e., moisture content, fuel type (i.e., grasses, woody debris), combustion phase, fuel mixtures, and vertically and spatially heterogeneous fuel beds).

As highlighted in the literature an alternative route to overcome the lack of pre-fire fuel and combustion completeness characterization is to directly determine the radiant heat released (Hardy *et al.* 2001; Wooster *et al.* 2005). Research to quantify radiant energy released have been conducted at satellite, field, and laboratory scales (Wooster et al. 2005; Kremens et al., 2013; Smith et al. 2013). Specifically, instantaneous measurements of fire radiative power (FRP, Units: Watts) has been demonstrated to be linearly related to the rate of biomass consumed (Kaufman, Kleidman, *et al.* 1998; Wooster *et al.* 2005). FRP is a

dynamic measurement that changes continuously with regards to fuel characteristics, environmental features, weather conditions, and fire's diurnal variability (Zhukov *et al.* 2006; Freeborn *et al.* 2008; Roberts *et al.* 2009; Kumar *et al.* 2011; Smith *et al.* 2013a). To estimate the total amount of biomass consumed across an affected landscape, FRP is integrated with time to calculate fire radiative energy (FRE, Unit: Joules), which is linearly related to total biomass consumed (Wooster *et al.* 2005). Three principal methods have been developed to estimate FRP that can be generally described as dual-band infrared thermometry, 4 μm radiance, and brightness temperature methods (Dozier 1981; Kaufman, Justice, *et al.* 1998). The strengths and weaknesses of these methods for satellite imagery are detailed in the literature (Wooster *et al.* 2003).

Although the assessment of biomass consumed from FRP and FRE are widely conducted, several studies have highlighted sources of uncertainty (Freeborn *et al.* 2008; Boschetti and Roy 2009; Kumar *et al.* 2011; Smith *et al.* 2013). Notably, errors can be introduced due to the nature of satellite systems with spatial and temporal undersampling that does not account for the natural variability of FRP (Boschetti and Roy 2009; Kumar *et al.* 2011). Despite our understanding of its complexity, studies have shown linear relationships between the FRP and the rate of biomass consumed (Wooster *et al.* 2005; Freeborn *et al.* 2008). Coarse spatial resolution satellite sensors have been demonstrated to underestimate FRP by as much as 50% due to their inability to detect pixels with little fire activity (Kumar *et al.* 2011),.

A further source of uncertainty on FRP estimates that has yet to be widely researched is the impacts of canopy closure (Freeborn et al. 2008). Specifically, within woodland and

forested systems, research is needed to assess the degree to which a thermal signal received at the sensor is attenuated by tree canopies. Specific questions we seek to address include:

1. What is the magnitude of FRP attenuation due to increases in tree canopy cover?
2. Do canopy characteristics such as living but non-transpiring versus desiccated, affect the relationship between emitted and observed power?

Methods

Experimental Setup

Laboratory experiments were conducted at the Idaho Fire Institute of Research and Education (IFIRE) lab located in Moscow Idaho to explore the influence of canopy cover on sensor observed radiant energy as suggested by Freeborn *et al.* (2008). The lab contains an indoor climate controlled burn chamber that allows for the reduction of environmental effects (Smith *et al.* 2013). To minimize potential micro-climate variations in temperature and humidity within the chamber, experimental measurements were replicated with both obscured canopy and non-canopy treatments. A constant heat source was produced using three propane burning ceramic heaters (ENERCO, Cleveland, OH, Serial #170700-09001001) mounted together with an area totaling 0.25 m^2 comprising approximately 20% of the ground instantaneous field of view of the radiometer. Given the experiment is evaluating relative magnitudes of radiative power and is comparing the ratio of obstructed to unobstructed; the heat source did not need to encompass the total area of the sensors field of view.

A total of 26 burns were conducted with two types of canopy; desiccated (n=14) and living/non-transpiring (n=12). Approximately 30 ponderosa pine (*Pinus ponderosa)* branches were cut on the day of the experiment and were stored not connected to water. An

additional set of cut branches collected as part of another experiment were stored in water and after 15 minutes were observed to have ceased transpiration. Desiccated ponderosa pine branches were also collected from pre-cut slash piles and were allowed to fully cure to ambient conditions before the experiment. During the experiment the branches were suspended between the heat source and the radiometer (Figure 2a). Ambient temperatures averaged 20 ºC and relative humidity averaged 40.5%. The experiments were performed over a continuous range of canopy percentages from 0 – 90%.

FRP was determined using a dual band radiometer (Dexter Research Center, Dexter, MI, Serial # ST60 DX-1001) (0.1–6.5 μm and 8–14 μm) with an effective field of view of 27° that was installed 2.44 meters at nadir above the heat source (Kremens *et al.* 2010). Measurements were recorded every 0.5 seconds and calibrated to watts using dual-band infrared thermometry (Dozier 1981). A hot wire anemometer was placed 1.12 meters above and centered over the heat source to measure wind speed as part of another experiment. Canopy and needle temperatures were measured using type K thermocouples, with interior leaf temperature measured by threading a thermocouple inside the leaf and exterior temperatures were measure by taping thermocouples to leaves.

Data Analysis

A white background was laid on the ground for contrast and hemispherical images were taken prior to each burn at nadir and later used to quantify the percentage of canopy cover obscuring the radiometers field of view. Hemispherical images were analyzed using the Hemiview software package (Delta-T Devices Ltd, Cambridge, UK) and canopy cover calculated based on the sensors field of view. Given the heat sources required time to achieve a relatively steady state of power output (Figure 1), only values within the

asymptote were used in the calculation of the ratio between obscured/unobscured datasets (Table 1). To determine whether individual data points were within the asymptote region, a non-linear least squares model was fit to the raw data:

$$\text{NLS: } Y = a - b\, e^{-c\,x} \qquad [1]$$

Where *a* is the approximate asymptote value, *b* is *a* – the intercept, $c = -(\log((a-y)/b))/x$, and *y* is the value of *y* at the steepest increase, and *x* is the value of *x* at *y*. Least squares models were fitted to the obscured and unobscured FRP data and the ratio of the asymptote values were then regressed in a linear model to canopy cover. The full linear model was:

$$Y_{ijk} = \mu + \rho_i + a_j + b_k + e_{ijk} \qquad [2]$$

Where *Yijk* is the *ratio of* sensor observed obscured to unobscured radiant power, μ grand mean, ρi is the effect for being in the *ith* group (canopy cover type), a_j is the random effect of temperature, b_k is the random effect of relative humidity, and e_{ijk} is the experimental error. A t-test with an alpha of 0.05 was performed on the normalized means (the ratio over the percent canopy cover) of the two canopy types to determine if there was a difference between the two groups. Under a no canopy scenario the power observed by the sensor was assumed to be 100% and therefore the intercept of the model was forced to one.

Results

Figure 1 illustrates the significant reduction in observed radiant power with increases in canopy obstruction, where at 75% canopy cover we observed over 50% reduction in radiant power at the sensor. Radiant power decreased at approximately 200 seconds after ignition on 63% of the obscured trials, whereas it remained steady for all unobscured runs. The canopy obscuration was reduced at lower canopy levels (Figure 1 b-d). Figure 2

demonstrates linear relationships between sensed FRP and canopy cover. A t-test performed on the normalized means (the ratio over the percent canopy cover) for non-transpiring green tree branches and desiccated tree branches showed that there was no significant difference between the two ($n=26$, $t=1.85$, p-value = 0.084). Our laboratory experiment did not show a statistically significant difference (alpha = 0.05) between the attenuation of radiant power between living non-transpiring and desiccated branches, which makes the developed correction factor applicable for a wide range of forest canopies, ranging from young and live to old canopies or canopies with beetle-killed branches. Specifically, Figure 3 illustrates the modeled reduction in rate of biomass consumed that would be observed under increasing canopy cover in surface fires occurring in mixed forest litter (Freeborn et al. 2008) and savannah woodlands with a grass understory (Wooster et al. 2005).

Discussion

Given proportional increases in FRP will likewise affect FRE these results could be extended to create correction factors for landscape-scale derived FRE estimates above woodland and forest canopies. With the increased availability of high spatial resolution satellite imagery and LiDAR derived canopy cover proxies; FRE corrections for canopy cover could be made with high precision at landscape scales. In areas without spatially explicit canopy measurements, landcover datasets such as are available from LANDFIRE or similar programs could be used for more generalized corrections of FRE. Under fire conditions which result in removal of canopy through torching or crowning, the use of pre-fire canopy data products could be misleading. In these cases, post-fire geospatial products such as aerial photography or fire severity maps that measure crown consumption could be consulted to eliminate a FRE correction being erroneously applied.

The decrease in observed power at approximately 200 seconds in Figure 1 (A, B, D) coincides with observed needle surface temperatures reaching between 45 and 60° C. We posit that this effect may be due to the epicuticle waxes of the needles melting (Tribmle *et al.* 1986), reducing the branches ability to regulate water flow and leading to increased amounts of water vapor entering the system. Also, the increased variability between the live and desiccated canopy groups can potentially be attributed to increased moisture content within the non-transpiring living branches (Vermote *et al.* 2009).

Conclusions

The specific questions we sought to address were: (1) What is the magnitude of FRP attenuation due to increases in tree canopy cover? and (2) Do canopy characteristics such as living but non-transpiring versus desiccated, affect the relationship between emitted and observed power? In terms of (1), we observed clear linear decreases in FRP as a result of simulated canopy cover increase. In terms of (2), although the variability increased within the living branches, no significant difference was observed between the live and dead branches.

This study provides a scalable method to correct for the bias introduced by the canopy's influence on radiant power reaching the sensor, which will in turn aid in the estimation of FRE and biomass consumed. At large-spatial scales application of leaf area index based products may provide a route to correct fire radiative power estimates. In addition to horizontal canopy cover, other factors will likely contribute to reductions in the observed FRP. Specifically, (i) height to live canopy may play a role in whether or not needle waxes melt under certain fire conditions; (ii) the structural stage of the forest (stem exclusion, multi-story, old growth, etc) will likely be a significant factor in how FRP is

attenuated; (iii) high LAI conditions (such as in tropical forests) may lead to very-high FRP attenuation during surface fires; and (iv) moisture content in both surface and canopy fuels (live/dead) will likely lead to further reductions in observed FRP (Smith et al. 2013). In summary, we suggest that the relationship developed here is an important step in understanding the energy balance for biomass burning that occurs under forested canopies.

References

Andreae MO, Merlet P (2001) Emission of trace gases and aerosols from biomass burning. *Biogeochemistry* **15**(4), 955–966.

Balch JK, Bradley B a., D'Antonio CM, Gómez-Dans J (2013) Introduced annual grass increases regional fire activity across the arid western USA (1980-2009). *Glob Chang Biol* **19**, 173–183. doi:10.1111/gcb.12046.

Barrett K, Kasischke ES (2013) Controls on variations in MODIS fire radiative power in Alaskan boreal forests: Implications for fire severity conditions. *Remote Sens Environ* **130**, 171–181. doi:10.1016/j.rse.2012.11.017.

Bartlett B, Schott J (2009) Atmospheric compensation in the presence of clouds: an adaptive empirical line method(AELM) approach. *J Appl Remote Sens* **3**, . doi:10.1117/1.3091937.

Boschetti L, Roy DP (2009) Strategies for the fusion of satellite fire radiative power with burned area data for fire radiative energy derivation. *J Geophys Res* **114**, . doi:D20302 10.1029/2008jd011645.

Bowman DMJS, Balch JK, Artaxo P, Bond WJ, Carlson JM, Cochrane M a, Antonio CMD, Defries RS, Doyle JC, Harrison SP, Johnston FH, Keeley JE, Krawchuk M a, Kull C a, Marston JB, Moritz M a, Prentice IC, Roos CI, Scott AC, Swetnam TW, Werf GR Van Der, Pyne SJ (2009) Fire in the Earth System. **324**(April), 481–484. doi:10.1126/science.1163886.

Crutzen PJ, Andreae MO (1990) Biomass burning in the tropics: impact on atmospheric chemistry and biogeochemical cycles. *Science* **250**(4988), 1669–1678. doi:10.1126/science.250.4988.1669.

Dozier J (1981) A method for satellite identification of surface temperature fields of subpixel resolution. *Remote Sens Environ* **11**, 221–229. doi:10.1016/0034-4257(81)90021-3.

Freeborn PH, Wooster MJ, Hao WM, Ryan CA, Nordgren BL, Baker SP, Ichoku C (2008) Relationships between energy release, fuel mass loss, and trace gas and aerosol emissions during laboratory biomass fires. *J Geophys Res* **113**(D1), . doi:D01301 10.1029/2007jd008679.

Ichoku C, Giglio L, Wooster MJ, Remer L a. (2008) Global characterization of biomass-burning patterns using satellite measurements of fire radiative energy. *Remote Sens Environ* **112**(6), 2950–2962. doi:10.1016/j.rse.2008.02.009.

Ichoku C, Kaufman YJ (2005) A method to derive smoke emission rates from MODIS fire radiative energy measurements. *IEEE Trans Geosci Remote Sens* **43**(11), 2636–2649. doi:10.1109/TGRS.2005.857328.

Jain a, Yang X, Kheshgi H, McGuire A, Post W, Kicklighter D (2009) Global Biogeochemical Cycles. *Global Biogeochem Cycles* **28**(11), 1295–1310. doi:10.1002/2013GB004679.Received.

Kaiser JW, Heil a., Andreae MO, Benedetti a., Chubarova N, Jones L, Morcrette J-J, Razinger M, Schultz MG, Suttie M, van der Werf GR (2012) Biomass burning emissions estimated with a global fire assimilation system based on observed fire radiative power. *Biogeosciences* **9**(1), 527–554. doi:10.5194/bg-9-527-2012.

Kaufman YJ, Justice CO, Flynn LP, Kendall JD, Prins EM, Giglio L, Ward DE, Menzel WP (1998) Potential global fire monitoring from EOS-MODIS. **103**(98), .

Kaufman YJ, Kleidman RG, King MD (1998) SCAR-B fires in the tropics: Properties and remote sensing from EOS-MODIS. *J Geophys Res*.

Kremens RL, Dickinson MB, Bova AS (2012) Radiant flux density , energy density and fuel consumption in mixed-oak forest surface fires. *Int J Wildl Fire* **21**(2008), 722–730.

Kremens RL, Smith AMS, Dickinson MB (2010) Fire metrology: current and future directions in physics-based methods. **6**(1), 13–35. doi:10.4996/fireecolo.

Kumar SS, Roy DP, Boschetti L, Kremens R (2011) Exploiting the power law distribution properties of satellite fire radiative power retrievals: A method to estimate fire radiative energy and biomass burned from sparse satellite observations. *J Geophys Res* **116**, . doi:D19303 10.1029/2011jd015676.

Van Lear DH, Carroll WD, Kapeluck PR, Johnson R (2005) History and restoration of the longleaf pine-grassland ecosystem: Implications for species at risk. *For Ecol Manage* **211**(1-2), 150–165. doi:10.1016/j.foreco.2005.02.014.

Loudermilk EL, Cropper JP, Mitchell RJ, Lee H (2011) Longleaf pine (Pinus palustris) and hardwood dynamics in a fire-maintained ecosystem: A simulation approach. *Ecol Modell* **222**(15), 2733–2750. doi:10.1016/j.ecolmodel.2011.05.004.

Parresol BR, Blake JI, Thompson AJ (2012) Effects of overstory composition and prescribed fire on fuel loading across a heterogeneous managed landscape in the southeastern USA. *For Ecol Manage* **273**, 29–42. doi:10.1016/j.foreco.2011.08.003.

Roberts G, Wooster MJ, Lagoudakis E (2009) Annual and diurnal african biomass burning temporal dynamics. *Biogeosciences* **6**(5), 849–866. <Go to ISI>://WOS:000266556300009.

Roberts G, Wooster MJ, Perry GLW, Drake N, Rebelo L-M, Dipotso F (2005) Retrieval of biomass combustion rates and totals from fire radiative power observations: Application to southern Africa using geostationary SEVIRI imagery. *J Geophys Res* **110**(D21), D21111. doi:10.1029/2005JD006018.

Roy DR, Boschetti L, Trigg SN (2006) Remote sensing of fire severity: Assesing the performance of the normalized Burn ratio. *Ieee Geosci Remote Sens Lett* **3**(1), 112–116. doi:10.1109/lgrs.2005.858485.

Smith AMS, Tinkham WT, Roy DP, Boschetti L, Kremens RL, Kumar SS, Sparks AM, Falkowski MJ (2013a) Quantification of fuel moisture effects on biomass consumed derived from fire radiative energy retrievals. *Geophys Res Lett* **40**(23), 6298–6302. doi:10.1002/2013GL058232.

Smith AMS, Tinkham WT, Roy DP, Boschetti L, Kremens RL, Kumar SS, Sparks AM, Falkowski MJ (2013b) Quantification of fuel moisture effects on biomass consumed derived from fire radiative energy retrievals. *Geophys Res Lett* **40**(23), 6298–6302. doi:10.1002/2013GL058232.

Smith AMS, Wooster MJ (2005) Remote classification of head and backfire types from MODIS fire radiative power and smoke plume observations. 249–254.

Thomas Caldwell Croker J (1987) LONGLEAF PINE A History of Man and a Forest. (Atlanta GA)

Thorsteinsson T, Magnusson B, Gudjonsson G (2011) Large wildfire in Iceland in 2006: Size and intensity estimates from satellite data. *Int J Remote Sens* **32**(1), 17–29. doi:10.1080/01431160903439858.

Tribmle JL, Skelly JM, Tolin SA, Orcutt DM (1986) Chemical and Structural Characterization of the Needle Epicuticular Wax of Two Clones of Pinus Strobus Differing in Sensitivity to Ozone. 652 – 656.

Vermote E, Ellicott E, Dubovik O, Lapyonok T, Chin M, Giglio L, Roberts GJ (2009) An approach to estimate global biomass burning emissions of organic and black carbon from MODIS fire radiative power. *J Geophys Res* **114**(D18), D18205. doi:10.1029/2008JD011188.

Vitousek PM, Aber JD, Howarth RW, Likens GE, Matson PA, Schindler DW, Schlesinger WH, Tilman DG (1997) Technical Report: Human Alteration of the Global Nitrogen Cycle: Sources and Consequences. *Ecol Appl* **7**(3), 727–750. doi:10.2307/2269431.

Westerling a L, Hidalgo HG, Cayan DR, Swetnam TW (2006) Warming and earlier spring increase western U.S. forest wildfire activity. *Science* **313**(August), 940–943. doi:10.1126/science.1128834.

Wooster MJ (2002) Small-scale experimental testing of fire radiative energy for quantifying mass combusted in natural vegetation fires. *Geophys Res Lett* **29**(21), 2027. doi:10.1029/2002GL015487.

Wooster MJ, Roberts G, Perry GLW, Kaufman YJ (2005) Retrieval of biomass combustion rates and totals from fire radiative power observations: FRP derivation and calibration relationships between biomass consumption and fire radiative energy release. *J Geophys Res* **110**(D24), . doi:D24311 10.1029/2005jd006318.

Wooster MJ, Zhukov B, Oertel D (2003) Fire radiative energy for quantitative study of biomass burning: derivation from the BIRD experimental satellite and comparison to MODIS fire products. *Remote Sens Environ* **86**(1), 83–107. doi:10.1016/s0034-4257(03)00070-1.

Wotton BM, Nock C a., Flannigan MD (2010) Forest fire occurrence and climate change in Canada. *Int J Wildl Fire* **19**, 253–271. doi:10.1071/WF09002.

Yokelson RJ, Burling IR, Gilman JB, Warneke C, Stockwell CE, De Gouw J, Akagi SK, Urbanski SP, Veres P, Roberts JM, Kuster WC, Reardon J, Griffith DWT, Johnson TJ, Hosseini S, Miller JW, Cocker DR, Jung H, Weise DR (2013) Coupling field and laboratory measurements to estimate the emission factors of identified and unidentified trace gases for prescribed fires. *Atmos Chem Phys* **13**, 89–116. doi:10.5194/acp-13-89-2013.

Zhukov B, Lorenz E, Oertel D, Wooster M, Roberts G (2006) Spaceborne detection and characterization of fires during the bi-spectral infrared detection (BIRD) experimental small satellite mission (2001–2004). *Remote Sens Environ* **100**(1), 29–51. doi:10.1016/j.rse.2005.09.019.

Table 1. The results from the models fit to the raw data measured by the radiometer given as obscured (unobscured) for each laboratory run. If there was no change in the relative humidity or temperature between runs then the previous unobscured run was used as the control.

Experiment Number	Estimate W m-2	Confidence Interval W m-2	
		Lower	Upper
Living 1	1110 (2552)	997 (2506)	1034 (2598)
Living 2	1893 (2617)	1876 (2599)	1909 (2635)
Living 3	1164 (2523)	1144 (2504)	1184 (2542)
Living 4	804 (2573)	773 (2555)	835 (2590)
Living 5	2274 (2485)	2257 (2462)	2290 (2507)
Living 6	794 (2485)	768 (2462)	820 (2507)
Living 7	1053 (2574)	1038 (2557)	1066 (2590)
Living 8	1095 (2491)	1072 (2474)	1117 (2508)
Living 9	1611 (2754)	1590 (2737)	1631 (2770)
Living 10	1793 (2513)	1781 (2495)	1804 (2529)
Living 11	512 (2550)	488 (2526)	535 (2576)
Living 12	1013 (2905)	997 (2890)	1027 (2920)
Desiccated 1	1743 (2631)	1731 (2605)	1755 (2657)
Desiccated 2	658 (2561)	666 (2546)	708 (2576)
Desiccated 3	1663 (2624)	1644 (2607)	1681 (2640)
Desiccated 4	929 (2633)	914 (2616)	945 (2648)
Desiccated 5	2526 (2677)	2512 (2663)	2539 (2694)
Desiccated 6	1324 (2526)	1308 (2512)	1339 (2539)
Desiccated 7	1147 (2526)	1131 (2512)	1162 (2539)
Desiccated 8	2652 (2879)	2614 (2843)	2692 (2913)
Desiccated 9	879 (2273)	853 (2234)	905 (2312)
Desiccated 10	2109 (2458)	2066 (2424)	2154 (2491)
Desiccated 11	2382 (2458)	2358 (2424)	2405 (2491)
Desiccated 12	1203 (2458)	1177 (2424)	1230 (2491)
Desiccated 13	1449 (3269)	1430 (3246)	1466 (3291)
Desiccated 14	2310 (3269)	2281 (3246)	2338 (3291)
Desiccated 15	2300 (2368)	2272 (2336)	2328 (2399)

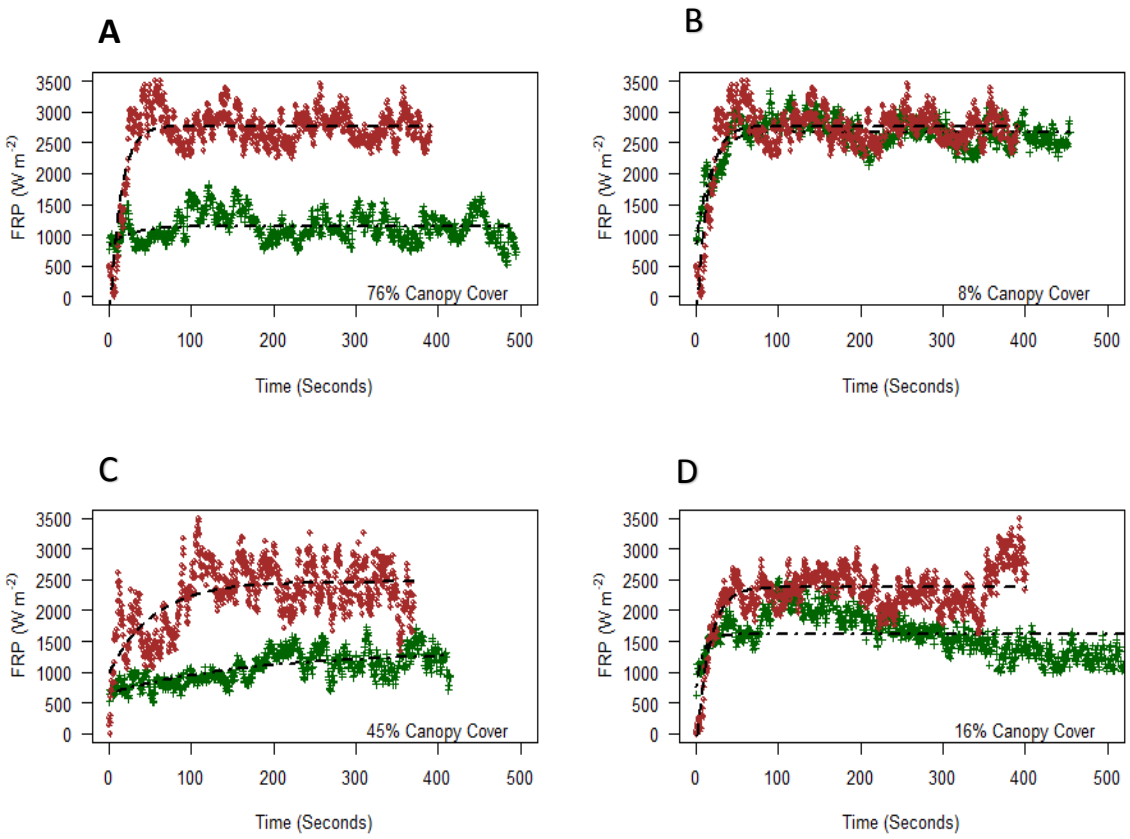

Figure 1. Calibrated data of FRP with temporal sampling every 0.5 seconds for four different canopy cover levels. Green points represent the obscured data, while brown represents the control. The fitted non-linear least squares model is shown as the dashed line for the control and dash-dot for the obscured data.

A

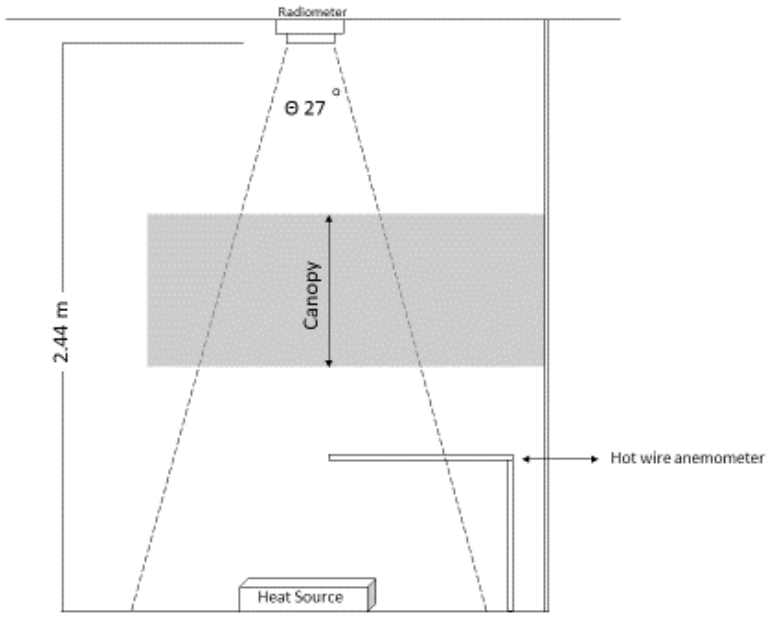

B

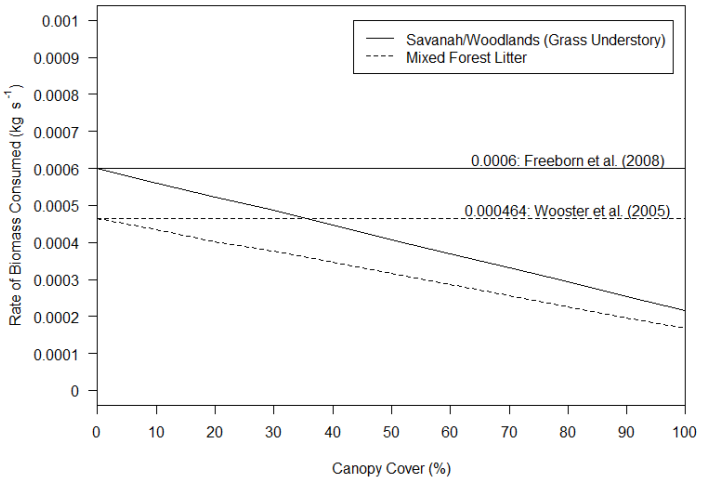

Figure 2. (A)Shows the laboratory experimental setup, while (B) shows the effects of canopy cover to the rate of biomass consumed under different surface fuels.

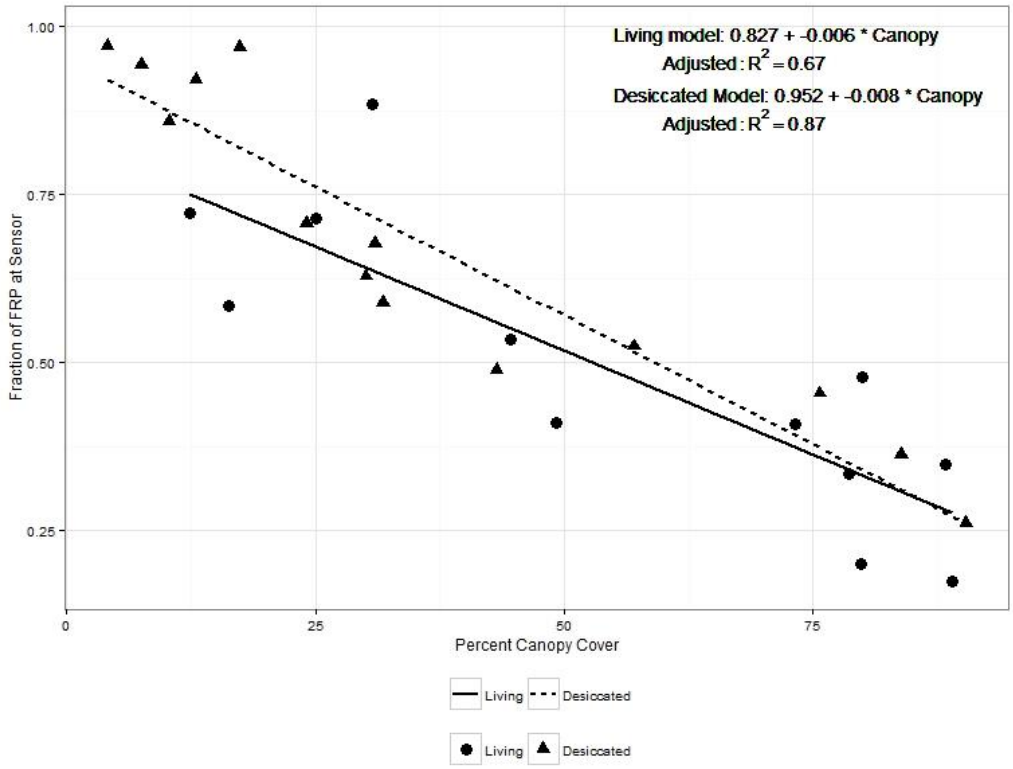

Figure 3. Effect of canopy obscuration on the sensor observed radiant energy. The regression was combined between canopy types given no significant difference between the two canopy cover types.

CHAPTER 2: ESTIMATING FIRE RADIATIVE ENERGY IN A LONGLEAF PINE FOREST FROM AIRBORNE THERMAL IMAGERY

Abstract

Airborne sensors are best suited for active fire remote sensing given the high spatial and temporal resolution needed to accurately characterize fire radiative power on the ground. In 2012, the Prescribed Fire Combustion and Atmospheric Dynamics Research Experiment (RxCADRE) sought to fill gaps in fire research through collecting a multidisciplinary suite of pre-, post- and active-fire measurements from a prescribed fire in Northwestern Florida. Here we use the unique data set collected by the RxCADRE team to estimate fire radiative energy (FRE) under a longleaf pine canopy using the wildfire airborne sensor program (WASP) sensor mounted on a fixed wing aircraft. Pre-fire LiDAR measurements quantified the forest canopy cover and surface fuels. Field measurement collected pre- and post-fire provided accurate estimates of the amount of biomass consumed by the prescribed fire. Through the canopy corrected estimates were we able to produce an acceptable estimate of total biomass consumption across the entire burned area. To reduce the underestimation that occurs due to canopy obscuration of FRE, we recommend that satellite based estimations implement a canopy correction when surface fires occur in a forested system.

Introduction

Fire radiative power (FRP) has been linked to the rate at which biomass is consumed during the combustion process, and FRP can be integrated over time to compute fire radiative energy (FRE) which is related to total biomass consumed through combustion

(Wooster *et al.* 2005). The link between FRE and the amount of biomass consumed, and thereafter the derived estimates for trace gas, particulate and aerosols production, has been widely studied by the remote sensing community since Kaufman *et al.* (1998) first explored the relationship. Understanding the details of this relationship is required if the atmospheric modeling community is to produce more accurate estimates of the role of fire in the interannual atmospheric carbon budget (Jain *et al.* 2009). Several studies have sought to better understand the physical relationship between FRE and biomass consumption and how fuel characteristics may play a role in observed FRE (Wooster 2002; Roberts *et al.* 2005; Kremens *et al.* 2010, 2012; Smith *et al.* 2013a). Localized experiments on individual fires have been used to estimate the amount of biomass consumed on a landscape scale or used to characterize ecological effects of the fire (Smith and Wooster 2005; Boschetti and Roy 2009; Thorsteinsson *et al.* 2011). Many studies have been conducted to characterize the amount of biomass consumption during fires on a global scale to better understand the interannual carbon budget (Ichoku *et al.* 2008; Vermote *et al.* 2009; Kaiser *et al.* 2012). All these efforts are focused on understanding the effects of biomass burning on terrestrial and atmospheric carbon.

Dozier (1981) first measured radiant energy by fitting data from the 3.7 and 11 μm bands of sensors onboard the geostationary orbiting environmental satellite (GOES) to a Planck function showing the possibility to estimate energy radiated from the Earth's surface. Significant advances in active fire remote sensing were seen from the launch of the Moderate Resolution Imaging Spectroradiometer (MODIS) sensor on the Earth Observation Satellite in 1999 and 2000 (Kaufman, Justice, *et al.* 1998; Kaufman, Kleidman, *et al.* 1998). Estimates of biomass consumption still could not be predicted from the radiant energy

products from MODIS, and therefore atmospheric scientists relied on environmental fire effects such as burned area for estimating emitted gas species (Ichoku and Kaufman 2005). Radiant energy released by a fire was known to be directly related to the amount of biomass consumed, but it was not until Wooster *et al.* (2005) that the linear relationship was experimentally demonstrated. Wooster *et al.* (2005) quantified the relationship of FRE to total consumed biomass using fuels and fuel characteristics, and their equation has been adjusted for fuel moisture to achieve a more accurate account of biomass consumption given fuel moisture levels (Smith *et al.* 2013a).

Image acquisition from polar orbiting satellites create their own challenges in the pursuit of estimating biomass consumption and trace gas emittance from active fires. The coarse spatiotemporal resolutions of images from sensors onboard polar orbiting satellites is such that they are unable to accurately capture the variability of FRP, which is needed to provide an accurate integration to FRE. Satellite sensors such as MODIS are typically used, sacrificing spatial resolution for higher temporal resolution. The reduced spatial resolution leads to the reduced ability to capture low intensity fires and the smoldering phase of combustion, which produces more emissions (Boschetti and Roy 2009; Barrett and Kasischke 2013).

Atmospheric chemistry influences the amount and range of the electromagnetic spectrum that reaches a sensor. Atmospheric transmissivity models such as Moderate Resolution Transmission (MODTRAN) use *in situ* measurements as parameters to quantify the absorption of given wavelengths from the electromagnetic spectrum by the atmosphere.

Approximately 28% of the global terrestrial lands are forested; with fire occurring from boreal to tropical ecosystems, forest fires account for a significant source of emissions to the atmosphere. Forested systems provide additional sources of error for estimations of FRP. Potential sources of error recognized by Freeborn *et al.* (2008) include environmental factors such as canopy cover and topography. These factors have yet to be studied but could have severe dampening effects of the FRP signal originating from surface fires, as observed from a satellite sensor.

In 2011 and 2012, the Prescribed Fire Combustion and Atmospheric Dynamics Research Experiment (RxCADRE) gathered a multidisciplinary team of 90 scientists and technicians to collect co-located information about pre-fire fuels, fire behavior, and post-fire effects. One goal of the RxCADRE project was to obtain fine scale measurements of FRP during prescribed fires to reproduce at a landscape scale the relationships between biomass consumption and observed radiative energy previously demonstrated at the scale of small burning experiments (Wooster *et al*. 2005, Smith *et al*. 2013, Ottmar *et al.* 2015).

During the fall of 2012, the RxCADRE team planned a prescribed fire in Northwestern Florida, on Eglin Air force base (Figure 1). Eglin contains the largest remaining contiguous stand of longleaf pine (*Pinus palustris*), encompassing roughly 146,500 hectares. Longleaf pine is a fire dependent ecosystem that historically has seen low to moderate severity fires with return intervals every 1-3 years; ignition sources came from both Native American practices and natural lighting strikes. Frequent fires reduced the chances of stand replacing fires by constantly maintaining low surface and ladder fuels, and created an environment that promoted a fire dependent ecosystem (Van Lear *et al.* 2005).

The distribution of longleaf pine savannah ecosystems at the time of European settlement ranged from Southeastern Virginia to Eastern Texas, encompassing over 35 million hectares. Longleaf pine was removed for plantations and was heavily logged to meet production and export needs of the 19th century, and were a much needed resource during WWI (Thomas Caldwell Croker 1987). Furthermore, due to the fire exclusion practices of the 20th century, longleaf pine stands have seen encroachment of hardwood species (Loudermilk *et al.* 2011). Today just over one million fragmented hectares remain. Eglin has a goal of burning over 28,000 hectares every year in their management of these fire dependent system of longleaf pine savannahs and coastal grasslands, which host over 77 rare species that thrive in fire dependent systems. Southeastern U.S. is unique in that it has a large window of opportunity for prescribed burning due to its climatic conditions, making it ideal for the logistics of successfully planning and implementing prescribed burns. The specific objectives of this study were to use the high spatiotemporal resolution imagery provided by the RxCADRE project to:

1) Determine the minimum number of FRP observations needed to estimate FRE.
2) Map fire radiative energy across a forested burn block with varying tree canopy cover and understory fuel loadings.

Methods

Study Area

The study area of interest was located on roughly 745 hectares with three burn blocks situated in Northwestern Florida on Eglin air force base (Figure 1). We focused on a 151 ha forested burn block (L2F) dominated by longleaf pine savannah (Ottmar *et al.* 2015). Fuel loadings surveyed on-site were similar to other studies of longleaf pine fuel beds that

experienced fire five years prior to measurements (Parresol *et al.* 2012, Ottmar *et al.* 2015b). Elevation of the L2F burn block ranged from 4.5 to 20 m above mean sea level. On the day of the burn, the relative humidity averaged 50 percent, and the mean temperature was 17° C.

Airborne data

A fixed wing aircraft from the Wildfire Airborne Sensor Program (WASP) utilized four Phoenix sensors and collected data over three infrared bands, short wave (0.9-1.7μm), middle wave (3.0-5.0μm), and long wave infrared (8.0-9.2μm) (Hudak *et al*. in review). The aircraft made multiple passes throughout the duration of the prescribed fire, which lasted for roughly three and a half hours. The sensor was able to collect an image, roughly 0.8 km x 1 km in extent with an average pixel size of 1.5 m x 1.5 m, every 3 seconds, and a total of 716 images were collected for L2F during the burn. Images were georectified based on the GPS system on the inertial measurement unit that accounts for the roll, pitch and yaw of the plane as the data are collected. Optical thickness of the atmosphere was measured pre-fire *in situ* from weather balloons and atmospheric transmission for given wavelengths were estimated from the MODTRAN radiative transfer model (Dickinson *et al.* in review). Images used the estimated transmissivity output by MODTRAN to correct for the effect of the atmosphere on the observed thermal signal (Bartlett and Schott 2009).

Field Measurements

Understory fuel inventories were collected prior to the prescribed burn; including pre-fire loadings by fuel classes on 30 (0.5 m X 0.5 m) clip quadrats within the L2F burn block, and 30 post-fire consumption plots measured along the same transects with alternating locations. Fuel classes included: grasses, forbs, shrubs, hardwood and conifer

litter, turkey oak (*Quercus cerris*), palmetto (*Serenoa repens*), 1000hr, 100hr, 10hr and 1hr fuels, litter and duff (Hudak *et al.* 2015).

Pre-fire fuels in the L2F burn block ranged from 2.0– 38.9 Mg ha^{-1} and averaged 8.9 Mg ha^{-1} prior to a correction to include duff, which increased the mean fuel load to 10.80 Mg ha^{-1}. The fuel loading was comparable to what other studies have found to be representative of longleaf pine stands that have burned approximately 3 - 5 years prior to measurements (Parresol *et al.* 2012). Post-fire consumption ranged from 0 – 95 % with an average of 58.9 %. Three highly instrumented plots (HIP) were located within the burn perimeter of L2F and contained a radiometer and an infrared camera. Another 72 0.5 m x 0.5 m clip plots recording pre-fire and post-fire fuels were located around 3 HIPs (Hudak et al. 2015). Fuel moistures were derived from five samples of each fuel class across the L2F burn block.

Pre-fire LiDAR data were collected on L2F and used to produce raster datasets of canopy characteristics and surface fuel loads. Mean canopy cover calculated from LiDAR for L2F was 37.3%. Surface fuels derived from LiDAR, averaged 6 kg m^{-1} with a minimum of 2 and a max of 16 kg m^{-1} (Hudak et al. 2015)

Analysis methods

Images were constrained to a threshold provided by *in situ* dual band radiometers that measured post-fire background radiant emittance (from a blackened surface) at 1070 W m^{-2}. By identifying an accurate background radiant emittance we reduced the bias that is typically associated with the mixing of smoldering and background radiation within a pixel that accounts for roughly 6% of FRE within a mixed smoldering and cooling pixel (Wooster

et al. 2003). Any pixel radiating above this threshold was considered a fire pixel, any pixel that was below the threshold was considered background noise or no fire present at sensor pass over. Complete time histories of radiant energy were extracted from every pixel that experienced fire and spatial references were maintained through time.

We compared the number of observations of four adjacent pixels to find the minimum number of FRP observations needed to integrate to FRE with reasonable accuracy. By choosing pixels located next to each other we could assume that fuel loadings should be similar, and therefore max values and distribution of FRP observations over time should be very similar across those pixels. The four selected pixels had 90, 67, 24, and 10 observations respectively. To aid our understanding of the error associated with a given number of observations a bootstrapping method was used on subsamples of a point with 127 observations. For each unique set of subsamples a 1,000 replicates were ran with mean and standard deviation recorded, and confidence intervals calculated for each set of subsamples.

The high temporal resolution of airborne imagery is well suited for pixel level integration of FRP to FRE as discussed in Boschetti and Roy (2009). This method assumes that the duration of the fire at that location is based on the first and last observation of the sensor. Integration to FRE was done using the trapezoidal method on all selected pixels. Biomass consumption estimates were calculated following the method described in Wooster *et al.* (2005), for the selected fire pixels.

Biomass combusted (kg) = 0.368 (± 0.015)* FRE (MJ) Equation 1

Each pixel was assigned a percent canopy cover based on the LiDAR derived product, and canopy cover correction of FRE was calculated given the methods from Chapter 1.

$$FRE_{cc}\ (MJ) = FRE_{obs} / (1 - 0.007\ (\pm\ 0.0016)*CC) \qquad \text{Equation 2}$$

Where FRE_{cc} is the canopy corrected FRE, FRE_{obs} is FRE integrated from observed FRP, and CC is the percent canopy cover for that pixel. Biomass consumption estimates were calculated from the corrected FRE values and compared to the uncorrected estimate of total biomass consumed for all given pixels.

Spatially discrete measurements of FRE were obtained for pixels selected from the minimum threshold of 10 observations. Following Boschetti and Roy (2009), we used a kriging method of interpolation across the burned area to compute total FRE for the entire L2F burn block. Kriging provides a linear estimate between two points with weighted averages of surrounding points. We used a spherical semi-variogram model and 12 surrounding points as inputs for the interpolation model. Kriging was performed on both pre- and post- canopy corrected FRE pixels.

Results

Image processing

Of the 716 images collected for L2F burn block, 568 of those images contained pixels that burned in the prescribed fire (Figure 2). The total unburned area was 26 of the 151 hectares, defined as all pixels that never received an observation that exceeded the 1070 W m^{-2} threshold.

Selection of minimum number of FRP observations per pixel

The comparison of the four fire pixels with different number of FRP observations, 90, 67, 24, 10 respectively, shows that all four pixels retained similar maximum FRP values along with a similar distribution of observations (Figure 3). Assuming the pixel with 90 observations capture 100 % of the energy released during the fire within that pixel, then the remaining pixels captured 80, 59, and 23 % of the total energy respectively. The bootstrapping was performed on a pixel with 127 observations, and 1,000 replicates provided the mean average FRE estimated from subsets of observations ranging from 5 to 120 (Table 1). We found that on average 10 observations captured 67 % of the total energy possible. A 95% confidence interval showed that 10 observations captured between 20 and 115 percent of the radiant energy (Table 1). By selecting pixels with at least 10 observations we would cover 38% of the total L2F burn block or 47 hectares. The error associated with each pixel used in discrete estimates of FRE is shown in Figure 4.

Integration to FRE

Integration from FRP to FRE was done using the trapezoidal method on all fire pixels with a minimum of 10 observations. FRE on the individual pixels was summarized to 812,497 MJ across the 47 hectares which translates to 299 Mg of biomass consumption according to equation 1 (Wooster et al. 2005). The total surface fuels available for consumption was 513 Mg from the area used for discrete FRE measurements. Pre-canopy corrected FRE estimated 58.3% consumption over the area. Canopy correction was performed based on equation 2, on the estimated FRE using the LiDAR product for percent canopy cover. The corrected FRE estimated 1,166,531 MJ across the 47 hectares which translates to 429.3 Mg of biomass consumed, equaling 83.6% consumption (Figure 5). Estimates of pre-corrected FRE are similar to those reported by Hudak et al. (2015), of

58.9% observed consumption that was measured *in situ* post fire, whereas the corrected consumption exceeds those observed by 24.7%.

The results from the kriging procedure reduced the percent consumption under both pre- and post-canopy corrected FRE. The total surface fuels available for consumption for the entire burned area was 1350 Mg. Pre-corrected FRE increased to 1,633,840 MJ from discrete estimates and the corrected FRE increased to 2,017,606 MJ across the entire burned area. This resulted in total biomass consumed for the L2F burn block at 601.3 and 873.9 Mg respectively and biomass consumption of 44.5% and 64.7% respectively (Table 2).

Discussion

Estimating FRE

With the discrete measurement of FRE we were able to accurately estimate the biomass consumption at 58.3% with the pre canopy-corrected estimates, compared to field measurements of 58.9% consumption. Post canopy-corrected estimates over-estimated biomass consumption by 24.7%. We conclude that the correction is accurately measuring the energy at discrete locations given that these areas may have higher fuel loads, comprised mainly of longleaf pine litter, compared to those where canopy cover is reduced (Parresol *et al.* 2012). Also Hudak et al. (2015) observed that large woody fuels may have been undersampled during the field data collection, which would add significant energy to the FRE estimate. Another factor that could be causing the higher estimate of biomass consumption when applying canopy-correction is the partial combustion of needles and branches within the canopy itself that occurred during the fire. Burn severity maps may be used to identify areas that experienced increased fire severity in terms of tree mortality. These areas could be masked from the canopy-correction to reduce biasing the estimate. In

the northeastern area of the burn block (see Figure 6), we see that the area experienced roughly a 90% increase in the amount of biomass consumed compared to the average of the burn block. This increase can be attributed to either torching of individual trees or crowning fire.

The high temporal resolution of the aerial thermal image acquisitions provided by the WASP system enabled capture of the peak power more precisely and with higher frequency than the typical sensors onboard polar orbiting satellites. Detailed information about the heating and cooling process enabled us to accurately estimate FRE for discrete locations within the burn unit. We were also able to record the energy release from the smoldering combustion and cooling process after the flaming fire front passed, which is typically lost due to the coarse spatial resolution of polar orbiting and geo-stationary satellites (Wooster *et al.* 2003). We were able to predict the amount of biomass consumed by the prescribed fire in the L2F forested burn block using kriging interpolation of FRE estimated from the airborne WASP sensor, compared to *in situ* field measurements of consumed biomass. Field consumption data estimated that 858.6 of the total 1350 Mg of biomass were consumed across the entire burned area of L2F. Canopy corrected estimated biomass consumed from the WASP sensor resulted in 873.9 Mg overestimating field measured consumption by 5.4%. The need to account for canopy in FRE estimates is evident in that pre canopy-corrected underestimated consumption by nearly 257.3 Mg, with 601.3 Mg of total consumed biomass or 44.5% consumption (Table 2).

The relationship between observed FRE and consumed biomass is also affected by the water content of the fuels, because the heating and evaporation of water in the fuels

consume energy. Therefore to achieve similar observed FRE measurements more biomass would need to be consumed as fuel moisture increases (Smith *et al.* 2013a). For example, estimating the water content of our fuels at 10% would increase our total biomass consumed from canopy corrected kriging estimate from 873.9 to 952.3 Mg. While this overestimates field measurements by 10.9% it was noted that field measurements may have undersampled large woody fuels. Furthermore, surface fuel consumption does not account for the biomass consumed by torching of tree canopies. Therefore, future studies may more accurately estimate the biomass consumed by the fire if fuel moisture measurements are available.

Temporal Sampling

Despite the similarities between maximum FRP values and distribution of observations given in Figure 3, we found that the use of the trapezoidal method of integration can lead to significant underestimation of FRE. Even under a high level of sampling with 90 observations over the duration of the fire in this particular location (~ 1.5 hours) the maximum FRP value was only observed once. Likewise dropping to 67 observations a single observation of maximum FRP was acquired, the next closest observation was ~ 4000 W m^{-2} lower than the max FRP observed (see Figure 3B). This confirms what is already known about the issues of temporal undersampling of satellite based methods for FRP estimation. We show in detail that it is very unlikely that peak power will be observed from a polar orbiting sensor (Roy *et al.* 2006; Kremens *et al.* 2010). While multiple observations of FRP were achieved at discrete location, FRE derived from minimal observations (n = 10) reduced the estimated FRE by as much as 80% (Table 1).

Conclusion

The need to accurately account for the amount of biomass consumed during wildfires is a necessity for the atmospheric modeling community and for a better understanding of the global carbon budget. This study has shown that given adequate spatiotemporal resolution imagery, it is possible to accurately estimate FRE and biomass consumption under varying canopy cover conditions. Unlike studies conducted with satellite data, the temporal resolution of data obtained from sensors mounted on an airplane was adequate to estimate discrete measurements of FRE giving reliable points for spatial interpolation. The methods described in Chapter 1 have proved to be a useful technique in correcting for canopy cover when estimating FRE in a forested system. Kriging proved to be a reliable method for interpolation from the discrete measurement despite the lack of data in the eastern portion of the burn block (see Figure 5).

To accurately estimate the amount of biomass consumed during a fire from FRE estimates, many factors needed to be accounted for outside of the spatiotemporal undersampling that is typical with current satellite based sampling methods. Here we have addressed the need to correct for the obscuration of radiant energy by a forest canopy, but fuel moisture, topography, fuel loading characteristics, and ground validation, as recognized by others, still need to be addressed (Freeborn *et al.* 2008; Kremens *et al.* 2010; Smith *et al.* 2013b).

References

Andreae MO, Merlet P (2001) Emission of trace gases and aerosols from biomass burning. *Biogeochemistry* **15**(4), 955–966.

Balch JK, Bradley B a., D'Antonio CM, Gómez-Dans J (2013) Introduced annual grass increases regional fire activity across the arid western USA (1980-2009). *Glob Chang Biol* **19**, 173–183. doi:10.1111/gcb.12046.

Barrett K, Kasischke ES (2013) Controls on variations in MODIS fire radiative power in Alaskan boreal forests: Implications for fire severity conditions. *Remote Sens Environ* **130**, 171–181. doi:10.1016/j.rse.2012.11.017.

Bartlett B, Schott J (2009) Atmospheric compensation in the presence of clouds: an adaptive empirical line method(AELM) approach. *J Appl Remote Sens* **3**, . doi:10.1117/1.3091937.

Boschetti L, Roy DP (2009) Strategies for the fusion of satellite fire radiative power with burned area data for fire radiative energy derivation. *J Geophys Res* **114**, . doi:D20302 10.1029/2008jd011645.

Bowman DMJS, Balch JK, Artaxo P, Bond WJ, Carlson JM, Cochrane M a, Antonio CMD, Defries RS, Doyle JC, Harrison SP, Johnston FH, Keeley JE, Krawchuk M a, Kull C a, Marston JB, Moritz M a, Prentice IC, Roos CI, Scott AC, Swetnam TW, Werf GR Van Der, Pyne SJ (2009) Fire in the Earth System. **324**(April), 481–484. doi:10.1126/science.1163886.

Crutzen PJ, Andreae MO (1990) Biomass burning in the tropics: impact on atmospheric chemistry and biogeochemical cycles. *Science* **250**(4988), 1669–1678. doi:10.1126/science.250.4988.1669.

Dozier J (1981) A method for satellite identification of surface temperature fields of subpixel resolution. *Remote Sens Environ* **11**, 221–229. doi:10.1016/0034-4257(81)90021-3.

Freeborn PH, Wooster MJ, Hao WM, Ryan CA, Nordgren BL, Baker SP, Ichoku C (2008) Relationships between energy release, fuel mass loss, and trace gas and aerosol emissions during laboratory biomass fires. *J Geophys Res* **113**(D1), . doi:D01301 10.1029/2007jd008679.

Ichoku C, Giglio L, Wooster MJ, Remer L a. (2008) Global characterization of biomass-burning patterns using satellite measurements of fire radiative energy. *Remote Sens Environ* **112**(6), 2950–2962. doi:10.1016/j.rse.2008.02.009.

Ichoku C, Kaufman YJ (2005) A method to derive smoke emission rates from MODIS fire radiative energy measurements. *IEEE Trans Geosci Remote Sens* **43**(11), 2636–2649. doi:10.1109/TGRS.2005.857328.

Jain a, Yang X, Kheshgi H, McGuire A, Post W, Kicklighter D (2009) Global Biogeochemical Cycles. *Global Biogeochem Cycles* **28**(11), 1295–1310. doi:10.1002/2013GB004679.Received.

Kaiser JW, Heil a., Andreae MO, Benedetti a., Chubarova N, Jones L, Morcrette J-J, Razinger M, Schultz MG, Suttie M, van der Werf GR (2012) Biomass burning emissions estimated with a global fire assimilation system based on observed fire radiative power. *Biogeosciences* **9**(1), 527–554. doi:10.5194/bg-9-527-2012.

Kaufman YJ, Justice CO, Flynn LP, Kendall JD, Prins EM, Giglio L, Ward DE, Menzel WP (1998) Potential global fire monitoring from EOS-MODIS. **103**(98), .

Kaufman YJ, Kleidman RG, King MD (1998) SCAR-B fires in the tropics: Properties and remote sensing from EOS-MODIS. *J Geophys Res*.

Kremens RL, Dickinson MB, Bova AS (2012) Radiant flux density , energy density and fuel consumption in mixed-oak forest surface fires. *Int J Wildl Fire* **21**(2008), 722–730.

Kremens RL, Smith AMS, Dickinson MB (2010) Fire metrology: current and future directions in physics-based methods. **6**(1), 13–35. doi:10.4996/fireecolo.

Kumar SS, Roy DP, Boschetti L, Kremens R (2011) Exploiting the power law distribution properties of satellite fire radiative power retrievals: A method to estimate fire radiative energy and biomass burned from sparse satellite observations. *J Geophys Res* **116**, . doi:D19303 10.1029/2011jd015676.

Van Lear DH, Carroll WD, Kapeluck PR, Johnson R (2005) History and restoration of the longleaf pine-grassland ecosystem: Implications for species at risk. *For Ecol Manage* **211**(1-2), 150–165. doi:10.1016/j.foreco.2005.02.014.

Loudermilk EL, Cropper JP, Mitchell RJ, Lee H (2011) Longleaf pine (Pinus palustris) and hardwood dynamics in a fire-maintained ecosystem: A simulation approach. *Ecol Modell* **222**(15), 2733–2750. doi:10.1016/j.ecolmodel.2011.05.004.

Parresol BR, Blake JI, Thompson AJ (2012) Effects of overstory composition and prescribed fire on fuel loading across a heterogeneous managed landscape in the southeastern USA. *For Ecol Manage* **273**, 29–42. doi:10.1016/j.foreco.2011.08.003.

Roberts G, Wooster MJ, Lagoudakis E (2009) Annual and diurnal african biomass burning temporal dynamics. *Biogeosciences* **6**(5), 849–866. <Go to ISI>://WOS:000266556300009.

Roberts G, Wooster MJ, Perry GLW, Drake N, Rebelo L-M, Dipotso F (2005) Retrieval of biomass combustion rates and totals from fire radiative power observations: Application to southern Africa using geostationary SEVIRI imagery. *J Geophys Res* **110**(D21), D21111. doi:10.1029/2005JD006018.

Roy DR, Boschetti L, Trigg SN (2006) Remote sensing of fire severity: Assesing the performance of the normalized Burn ratio. *Ieee Geosci Remote Sens Lett* **3**(1), 112–116. doi:10.1109/lgrs.2005.858485.

Smith AMS, Tinkham WT, Roy DP, Boschetti L, Kremens RL, Kumar SS, Sparks AM, Falkowski MJ (2013a) Quantification of fuel moisture effects on biomass consumed derived from fire radiative energy retrievals. *Geophys Res Lett* **40**(23), 6298–6302. doi:10.1002/2013GL058232.

Smith AMS, Tinkham WT, Roy DP, Boschetti L, Kremens RL, Kumar SS, Sparks AM, Falkowski MJ (2013b) Quantification of fuel moisture effects on biomass consumed derived from fire radiative energy retrievals. *Geophys Res Lett* **40**(23), 6298–6302. doi:10.1002/2013GL058232.

Smith AMS, Wooster MJ (2005) Remote classification of head and backfire types from MODIS fire radiative power and smoke plume observations. 249–254.

Thomas Caldwell Croker J (1987) LONGLEAF PINE A History of Man and a Forest. (Atlanta GA)

Thorsteinsson T, Magnusson B, Gudjonsson G (2011) Large wildfire in Iceland in 2006: Size and intensity estimates from satellite data. *Int J Remote Sens* **32**(1), 17–29. doi:10.1080/01431160903439858.

Tribmle JL, Skelly JM, Tolin SA, Orcutt DM (1986) Chemical and Structural Characterization of the Needle Epicuticular Wax of Two Clones of Pinus Strobus Differing in Sensitivity to Ozone. 652 – 656.

Vermote E, Ellicott E, Dubovik O, Lapyonok T, Chin M, Giglio L, Roberts GJ (2009) An approach to estimate global biomass burning emissions of organic and black carbon from MODIS fire radiative power. *J Geophys Res* **114**(D18), D18205. doi:10.1029/2008JD011188.

Vitousek PM, Aber JD, Howarth RW, Likens GE, Matson PA, Schindler DW, Schlesinger WH, Tilman DG (1997) Technical Report: Human Alteration of the Global Nitrogen Cycle: Sources and Consequences. *Ecol Appl* **7**(3), 727–750. doi:10.2307/2269431.

Westerling a L, Hidalgo HG, Cayan DR, Swetnam TW (2006) Warming and earlier spring increase western U.S. forest wildfire activity. *Science* **313**(August), 940–943. doi:10.1126/science.1128834.

Wooster MJ (2002) Small-scale experimental testing of fire radiative energy for quantifying mass combusted in natural vegetation fires. *Geophys Res Lett* **29**(21), 2027. doi:10.1029/2002GL015487.

Wooster MJ, Roberts G, Perry GLW, Kaufman YJ (2005) Retrieval of biomass combustion rates and totals from fire radiative power observations: FRP derivation and calibration relationships between biomass consumption and fire radiative energy release. *J Geophys Res* **110**(D24), . doi:D24311 10.1029/2005jd006318.

Wooster MJ, Zhukov B, Oertel D (2003) Fire radiative energy for quantitative study of biomass burning: derivation from the BIRD experimental satellite and comparison to MODIS fire products. *Remote Sens Environ* **86**(1), 83–107. doi:10.1016/s0034-4257(03)00070-1.

Wotton BM, Nock C a., Flannigan MD (2010) Forest fire occurrence and climate change in Canada. *Int J Wildl Fire* **19**, 253–271. doi:10.1071/WF09002.

Yokelson RJ, Burling IR, Gilman JB, Warneke C, Stockwell CE, De Gouw J, Akagi SK, Urbanski SP, Veres P, Roberts JM, Kuster WC, Reardon J, Griffith DWT, Johnson TJ, Hosseini S, Miller JW, Cocker DR, Jung H, Weise DR (2013) Coupling field and laboratory measurements to estimate the emission factors of identified and unidentified trace gases for prescribed fires. *Atmos Chem Phys* **13**, 89–116. doi:10.5194/acp-13-89-2013.

Zhukov B, Lorenz E, Oertel D, Wooster M, Roberts G (2006) Spaceborne detection and characterization of fires during the bi-spectral infrared detection (BIRD) experimental small satellite mission (2001–2004). *Remote Sens Environ* **100**(1), 29–51. doi:10.1016/j.rse.2005.09.019.

Table 1. Error associated with the number of observations given the assumed total energy, 47.16 (MJ), by the pixel with the highest number of observations (127). Confidence intervals for the energy estimated along with the percent of total energy estimated.

Point Id = 2165414	n =127	FRE (MJ) = 47.16		Confidence Int. (MJ)		% Est. Confidence	
Observations	Mean (MJ)	Std. Dev	% Energy Capturing	lower	upper	lower	upper
n=5	24.4	15.5	51.7	0	55	0	116
n=10	31.74	11.5	67.3	9	54	20	115
n=20	36.98	7.89	78.4	22	52	46	111
n=30	39.57	6.33	83.9	27	52	58	110
n=40	40.68	5.22	86.3	30	51	65	108
n=50	41.69	4.28	88.4	33	50	71	106
n=60	42.74	3.65	90.6	36	50	75	106
n=70	43.86	3.12	93.0	38	50	80	106
n=80	44.31	2.7	94.0	39	50	83	105
n=90	45.14	2.34	95.7	41	50	86	105
n=100	45.8	2.04	97.1	42	50	89	106
n=110	46.5	1.64	98.6	43	50	92	105
n=120	46.95	1.06	99.6	45	49	95	104

Table 2. Summary of the results from the integration to FRE and the block wide FRE estimates from kriging interpolation. Biomass consumptions are all reported following Wooster *et al*. (2005) and are very similar to those measured in the field (58.9) Hudak et al. (2015). Biomass was calculated across the burn block using average field measurements. Total biomass available for consumption for total burned area is 1,350,000 kg and 513,000 kg for the discrete measurements of FRE.

	FRE (MJ) (Discrete Measurements)	FRE (MJ) (Kriging Interpolation)	Biomass Consumption (Mg) (Discrete)	Biomass Consumption (Mg) (Kriging)	Percent Consumed Discrete (Kriging)
Pre-Correction	812,497	1,633,840	298.9	601.3	58.3 (44.5)
Post-Correction	1166531	2,374,757	429.3	873.9	83.6 (64.7)

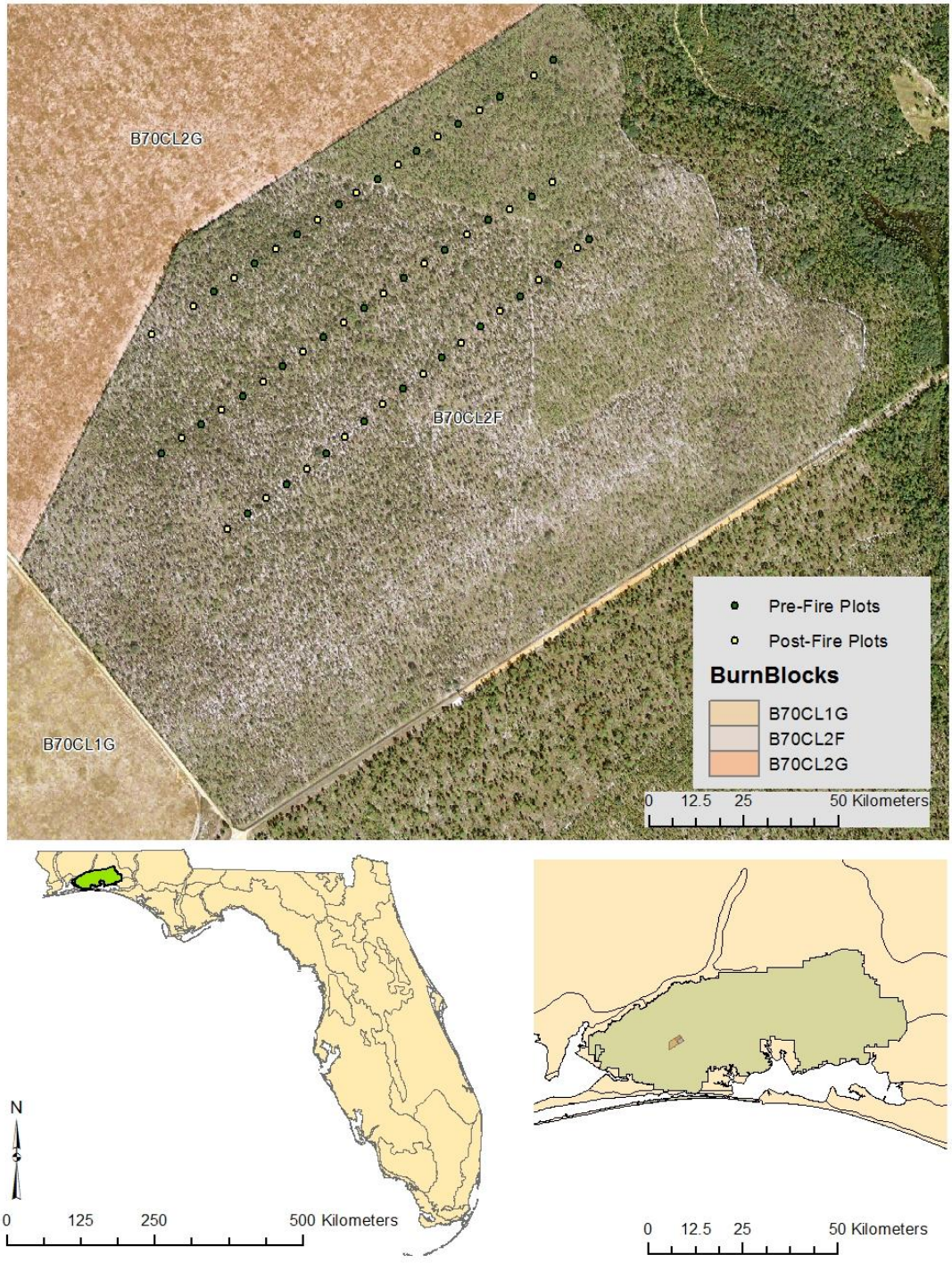

Figure 1. Study area map of Eglin air force base in Northwestern Florida with clip plots for collecting fuel data.

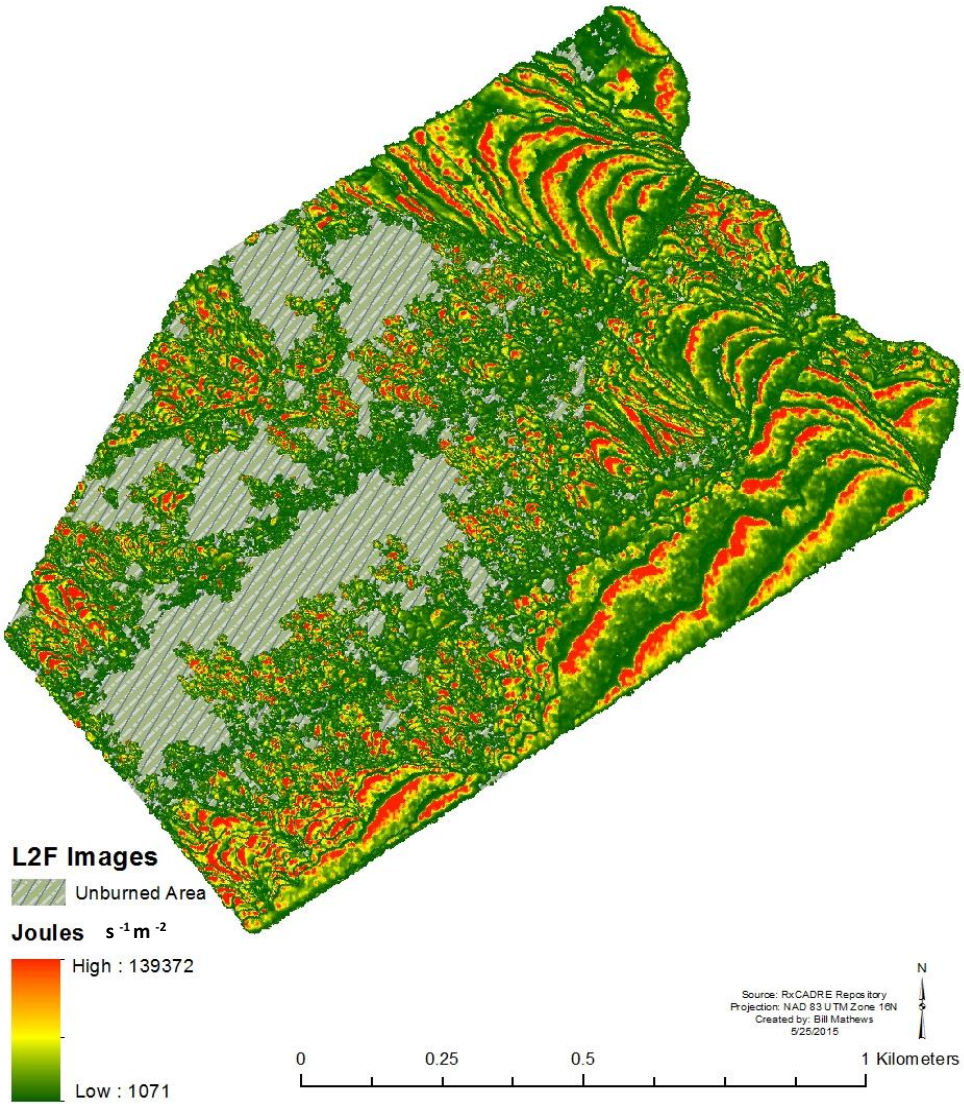

Figure 2. L2F forested plot with all 568 images containing at least one fire pixel. The green hatched area represents the unburned portion of the L2F burn block. No FRP observations were recorded in these pixels during the time of the burn and we assume that those pixels were unburned.

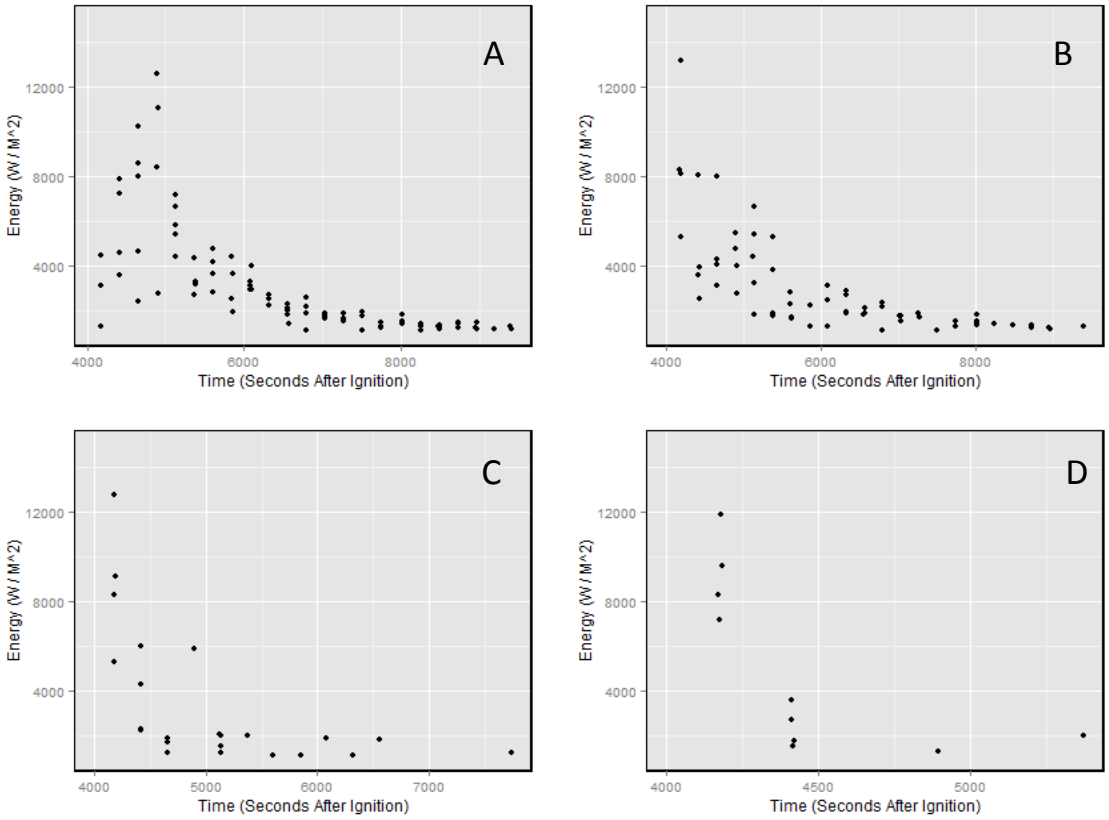

Figure 3. Complete time histories of four adjacent pixels with different number of observations recorded by the WASP sensor. (A) Pixel with a total of 90 observations and shows the entire heat up and cool down period of the fire. (B) Pixel with had a total of 67 observations which retains a similar distribution to (A). (C) A pixel with 24 observations loses some of the initial heat up and the length of the cool down time observed in (A). (D) A pixel with 10 observations keeps a similar maximum value but loses much of the heat up and cool down period of the fire. Integrating to FRE (in Mega Joules) using the trapezoidal method of integrating gave 13.33, 10.76, 7.9, and 3.1 (MJ m-2) for pixels A, B, C, and D respectively.

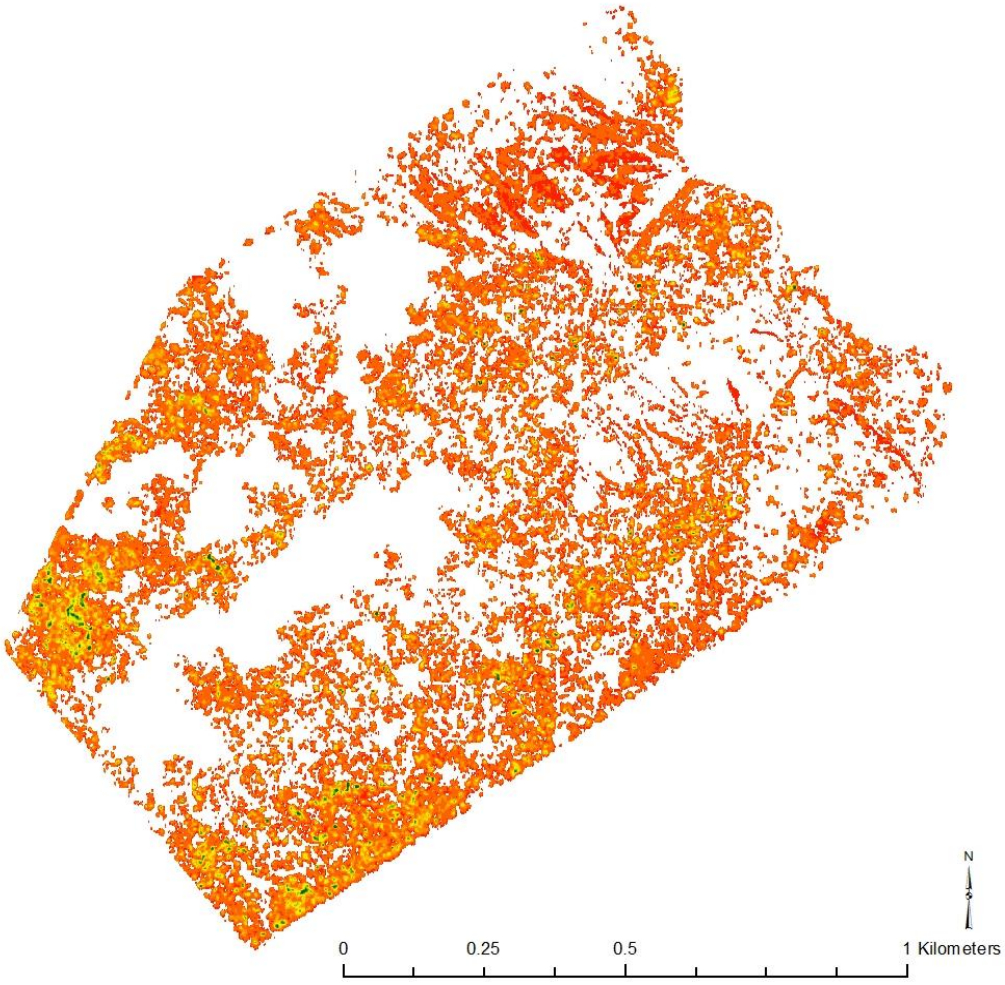

Confidence Intervals for Number of Observations

Number of Observations	Mean Estiamte (MJ)	Confidence Interval (MJ)	Number of Observations	Mean Estiamte (MJ)	Confidence Interval (MJ)
10	32	9 - 54	51 - 60	42	34 - 50
11 - 20	34	15 - 53	61 - 70	43	37 - 50
21 - 30	39	25 - 52	71 - 80	44	38 - 50
31 - 40	40	28 - 52	81 - 90	45	40 - 50
41 - 50	41	31 - 51	91 - 127	46	42 - 50

Figure 4. Map of the error associated with each point based on the number of observations made by the WASP sensor, total possible energy is 47.16 (MJ m-2). Confidence Intervals are based on subsampling a point with 127 observations over the duration of the fire.

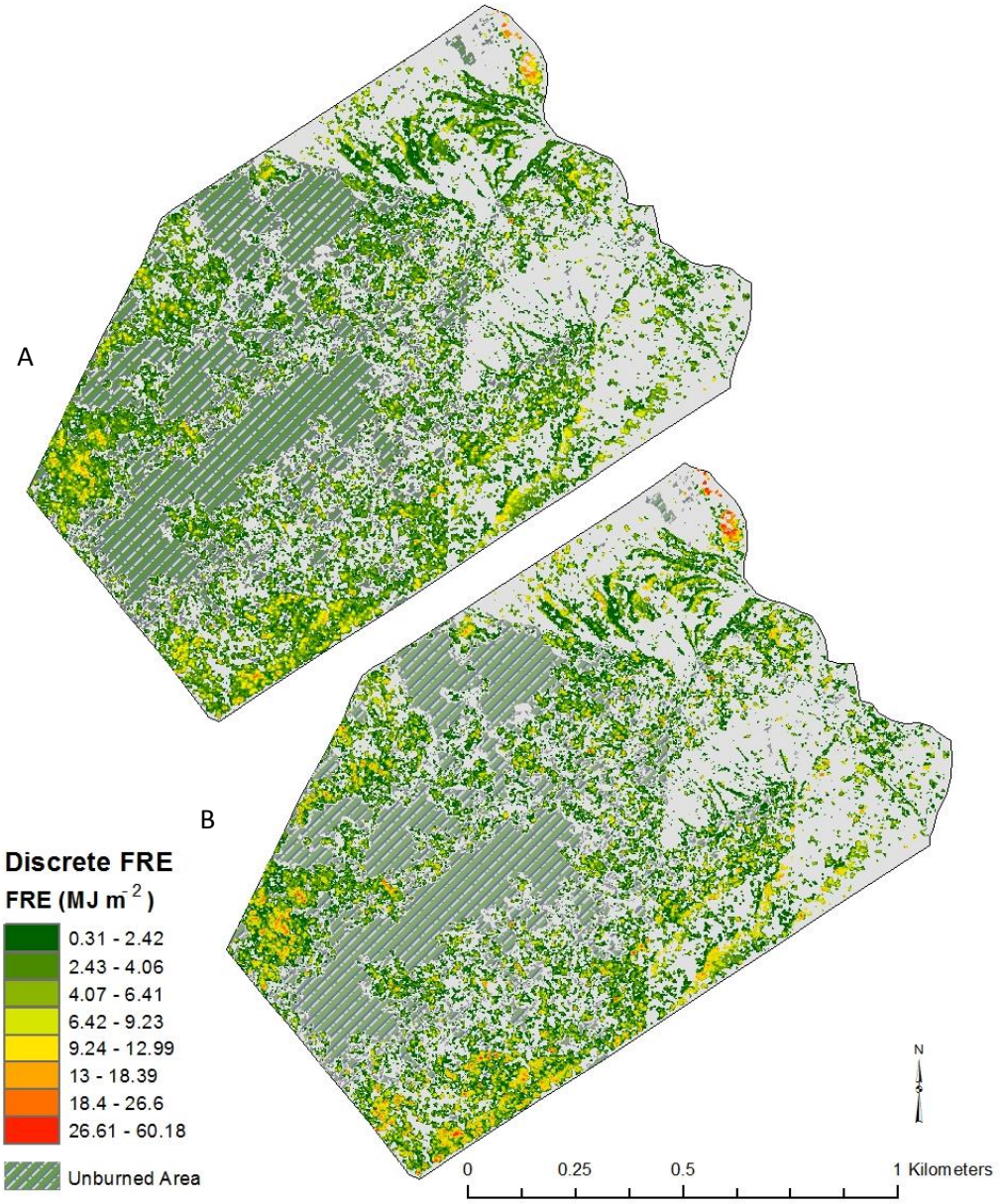

Figure 5. Map of FRE for pre-canopy correction, (A) and (B) along with post canopy correction. Total increase between pre and post correction was 354.1 MJ which resulted in an increase in biomass consumed by 130.3 Mg.

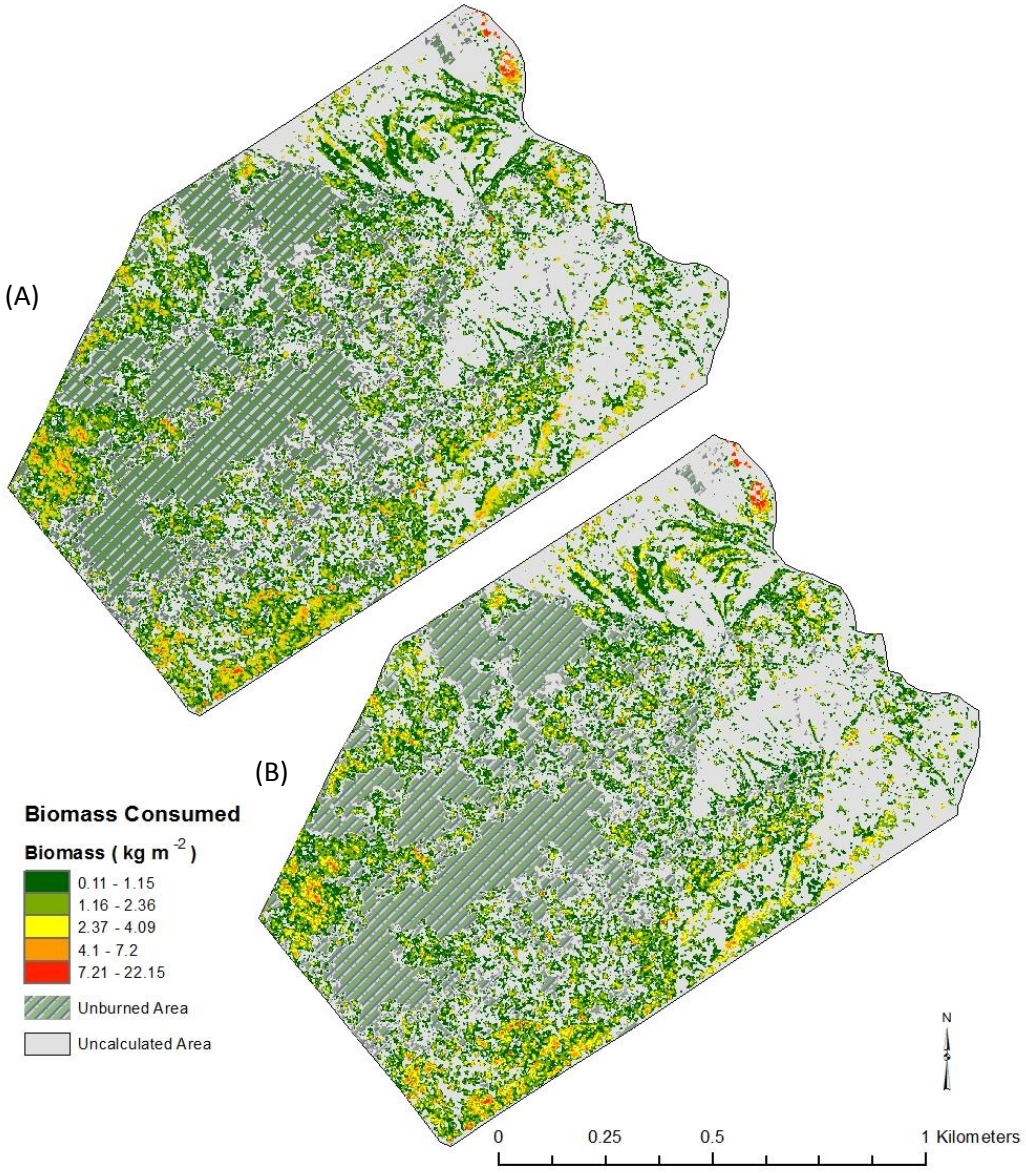

Figure 6. Estimation of biomass consumption for (A) uncorrected and (B) canopy corrected using Wooster et al.'s (2005) conversion between FRE and consumed biomass. The canopy correction increased the amount of biomass consumed by 130.3 Mg across the 47 hectares. Most apparent changes occur in extremely high valued areas from the uncorrected image.

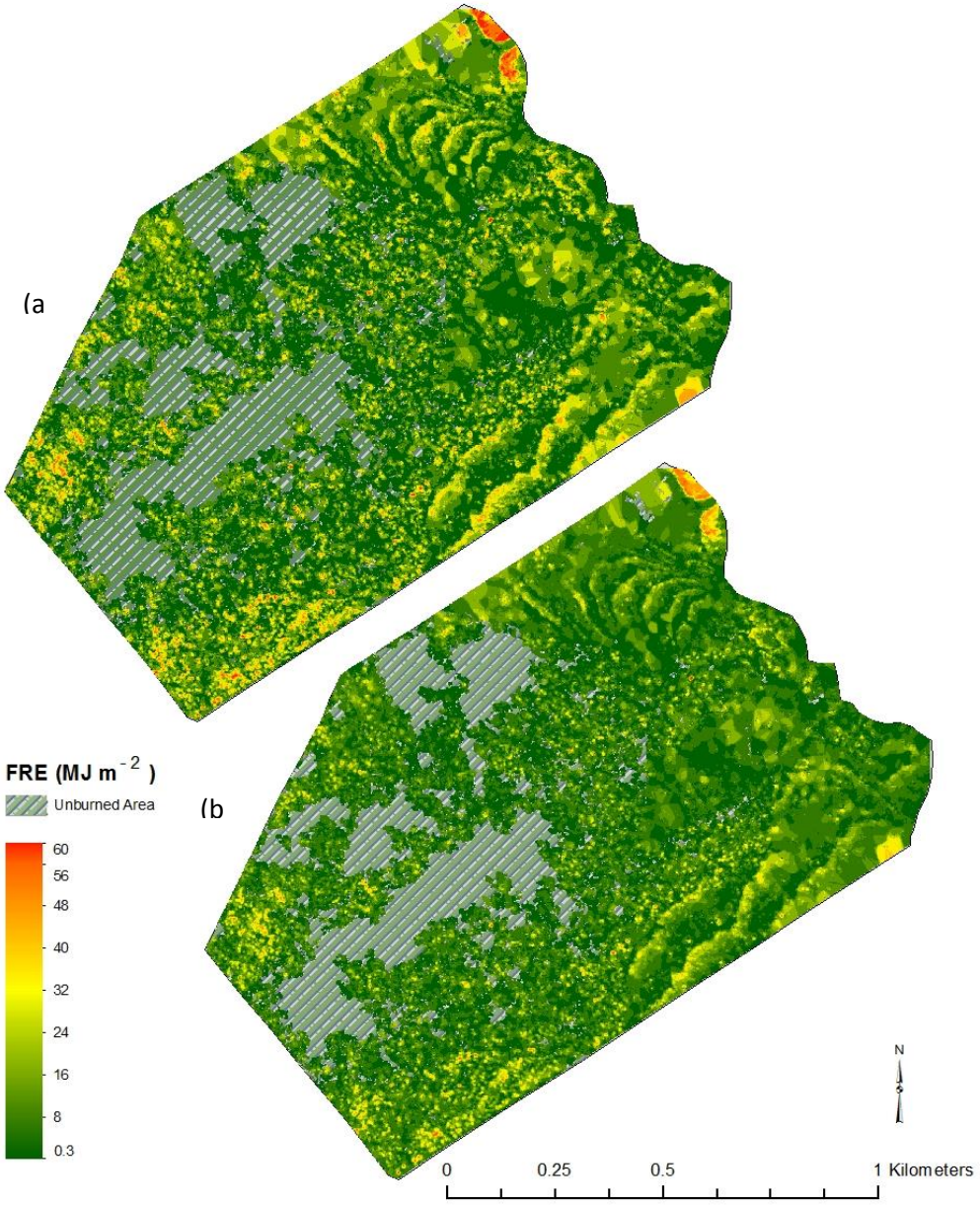

Figure 7. Map of the Kriging interpolation for both (a) pre and (b) post canopy corrected FRE estimates. It is difficult to see the degree of change at the plot level. The difference in FRE is 1,633.8 and 2,374.8 MJ respectively which resulted in a difference of 272.6 Mg of biomass consumed.

Appendix A

R-Code for Statistical Analysis of Laboratory Data

Fitting a Non-Linear Least Squares Model to Find the Average Asymptote

```
data <- read.csv("H:\\Cali_All.csv", header = T)

### a = approx. asymptot, b = a - intercept, c = c= -log((a-y)/b)/x where y is the steepest part of curve and x is x value under y

modelcc<-nls(data = data, Green_Nine ~ a-b*exp(-c*Time), start = list(a=1200,b=200,c=0.06931), control=nls.control(maxiter=200))
modelnb <- nls(data = data, Green_NineNB ~ a-b*exp(-c*Time), start = list(a=2700, b=1700, c=0.0318), control=nls.control(maxiter=200))
confint(modelcc)
confint(modelnb)
summary(modelcc)
summary(modelnb)
```

Fitting Linear Models to Canopy Cover and Fraction of Sensor Reaching FRP

```
green <- read.csv("H:\\Moscow_CanopyObscuration\\Outputs\\Green.csv", header = T)
des <- read.csv("H:\\Moscow_CanopyObscuration\\Outputs\\Desiccated.csv", header = T)

intercept <- 1.0
fit <- lm(I(MW.Ratio - intercept) ~ 0 + X..Cover, green)
fit2 <- lm(I(MW.Ratio - intercept) ~ 0 + X..Cover, des)
summary(fit)
summary(fit2)
```

Appendix B

R-Code for Analysis of Field Data Collected from RxCADRE

Reordering Data for Analysis

```
L2F_first <- read.csv("H:\\RxCADRE_L2F_2012\\Excel\\Quart1.csv", header = T)
L2F_second <- read.csv("H:\\RxCADRE_L2F_2012\\Excel\\Quart2.csv", header = T)
L2F_third <- read.csv("H:\\RxCADRE_L2F_2012\\Excel\\Quart3.csv", header = T)
L2F_fourth <- read.csv("H:\\RxCADRE_L2F_2012\\Excel\\Quart4.csv", header = T)

L2F_first <- L2F_first[,c(3:574)]
L2F_second <- L2F_second[,c(3:574)]
L2F_third <- L2F_third[,c(3:574)]
L2F_fourth <- L2F_fourth[,c(3:574)]

mask1 <- subset(L2F_first, count == 0)
mask2 <- subset(L2F_second, count == 0)
mask3 <- subset(L2F_third, count == 0)
mask4 <- subset(L2F_fourth, count == 0)
mask <- rbind(mask1,mask2,mask3,mask4)
write.csv(mask, file = "F:\\RxCADRE_L2F_2012\\Excel\\Mask.csv")

newl2f1 <- subset(L2F_first, count >= 10)
newl2f2 <- subset(L2F_second, count >= 10)
newl2f3 <- subset(L2F_third, count >= 10)
newl2f4 <- subset(L2F_fourth, count >= 10)

newl2fmelt1 <- melt(newl2f1, id.vars = c("pointid", "count", "POINT_X", "POINT_Y"))
names(newl2fmelt1)[names(newl2fmelt1) == 'variable'] <- 'time'
newl2fmelt2 <- melt(newl2f2, id.vars = c("pointid","count", "POINT_X", "POINT_Y"))
names(newl2fmelt2)[names(newl2fmelt2) == 'variable'] <- 'time'
newl2fmelt3 <- melt(newl2f3, id.vars = c("pointid","count", "POINT_X", "POINT_Y"))
names(newl2fmelt3)[names(newl2fmelt3) == 'variable'] <- 'time'
newl2fmelt4 <- melt(newl2f4, id.vars = c("pointid","count", "POINT_X", "POINT_Y"))
names(newl2fmelt4)[names(newl2fmelt4) == 'variable'] <- 'time'

newl2fmelt1$time <- gsub("X", "", newl2fmelt1$time)
newl2fmelt1$time <- gsub(".", ":", newl2fmelt1$time, fixed = T)
newl2fmelt1$time <- strptime(newl2fmelt1$time, "%H:%M:%S")
newl2fmelt1$time <- as.POSIXct(newl2fmelt1$time)
newl2fmelt1$pointid <- as.factor(newl2fmelt1$pointid)
newl2fmelt2$time <- gsub("X", "", newl2fmelt2$time)
newl2fmelt2$time <- gsub(".", ":", newl2fmelt2$time, fixed = T)
newl2fmelt2$time <- strptime(newl2fmelt2$time, "%H:%M:%S")
newl2fmelt2$time <- as.POSIXlt(newl2fmelt2$time)
newl2fmelt2$pointid <- as.factor(newl2fmelt2$pointid)
newl2fmelt3$time <- gsub("X", "", newl2fmelt3$time)
newl2fmelt3$time <- gsub(".", ":", newl2fmelt3$time, fixed = T)
newl2fmelt3$time <- strptime(newl2fmelt3$time, "%H:%M:%S")
```

```
newl2fmelt3$time <- as.POSIXlt(newl2fmelt3$time)
newl2fmelt3$pointid <- as.factor(newl2fmelt3$pointid)
newl2fmelt4$time <- gsub("X", "", newl2fmelt4$time)
newl2fmelt4$time <- gsub(".", ":", newl2fmelt4$time, fixed = T)
newl2fmelt4$time <- strptime(newl2fmelt4$time, "%H:%M:%S")
newl2fmelt4$time <- as.POSIXlt(newl2fmelt4$time)
newl2fmelt4$pointid <- as.factor(newl2fmelt4$pointid)

start_time <- newl2fmelt1$time[1]
newl2fmelt1$seconds <- start_time - newl2fmelt1$time
newl2fmelt1$seconds <- as.numeric(newl2fmelt1$seconds*-1)
start_time2 <- newl2fmelt2$time[1]
newl2fmelt2$seconds <- start_time2 - newl2fmelt2$time
newl2fmelt2$seconds <- as.numeric(newl2fmelt2$seconds*-1)
start_time3 <- newl2fmelt3$time[1]
newl2fmelt3$seconds <- start_time3 - newl2fmelt3$time
newl2fmelt3$seconds <- as.numeric(newl2fmelt3$seconds*-1)
start_time4 <- newl2fmelt4$time[1]
newl2fmelt4$seconds <- start_time4 - newl2fmelt4$time
newl2fmelt4$seconds <- as.numeric(newl2fmelt4$seconds*-1)

sub_new1 <- (newl2fmelt1[sample(which(newl2fmelt1$value >0)),])
ordered1 <- (sub_new1[order(sub_new1$seconds),])
sub_new2 <- (newl2fmelt2[sample(which(newl2fmelt2$value >0)),])
ordered2 <- (sub_new2[order(sub_new2$seconds),])
sub_new3 <- (newl2fmelt3[sample(which(newl2fmelt3$value >0)),])
ordered3 <- (sub_new3[order(sub_new3$seconds),])
sub_new4 <- (newl2fmelt4[sample(which(newl2fmelt4$value >0)),])
ordered4 <- (sub_new4[order(sub_new4$seconds),])

point_1 <- newl2fmelt4[newl2fmelt4$pointid == 3843884,]
point1 <- newl2fmelt1[newl2fmelt1$pointid == 2236726,]
point2 <- newl2fmelt1[newl2fmelt1$pointid == 2236727,]
point3 <- newl2fmelt1[newl2fmelt1$pointid == 2236728,]
point4 <- newl2fmelt1[newl2fmelt1$pointid == 2236729,]
point5 <- newl2fmelt1[newl2fmelt1$pointid == 2236790,]
```

Integrating FRP to FRE and Bootstrapping FRP Subsamples

```
set.seed(5)
sample = NULL
mn = NULL
repeat{
  sub_sample <- (point_1[ sample( which(point_1$value> 1070), 20), ])
  new_sample <- sub_sample[order(sub_sample$seconds),]
  a <- trapz(new_sample$seconds, new_sample$value)
```

```
  sample <- append(sample,a)
  mn <- append(mn, mean(sample))
  plot(new_sample$seconds, new_sample$value, type= "l")
  len <- length(sample)
  if (len > 10)
    break;
}

mean(sample)
sd(sample)

points1 <- split(ordered1, ordered1$pointid, drop = FALSE)
points2 <- split(ordered2, ordered2$pointid, drop = FALSE)
points3 <- split(ordered3, ordered3$pointid, drop = FALSE)
points4 <- split(ordered4, ordered4$pointid, drop = FALSE)

FRE1 <- NULL
FRE2 <- NULL
FRE3 <- NULL
FRE4 <- NULL
id <- unique(newl2fmelt1$pointid)
id2 <- unique(newl2fmelt2$pointid)
id3 <- unique(newl2fmelt3$pointid)
id4 <- unique(newl2fmelt4$pointid)

for (i in points1){
  FRE_1 <- trapz(i$seconds, i$value)
  #print(FRE_1)
  FRE1 <- append(FRE1,FRE_1)
}
for (i2 in points2){
  FRE_2 <- trapz(i2$seconds, i2$value)
  #print(FRE_2)
  FRE2 <- append(FRE2,FRE_2)
}
for (i3 in points3){
  FRE_3 <- trapz(i3$seconds, i3$value)
  #print(FRE_3)
  FRE3 <- append(FRE3,FRE_3)
}
for (i4 in points4){
  FRE_4 <- trapz(i4$seconds, i4$value)
  print(FRE_4)
  FRE4 <- append(FRE4,FRE_4)
}
```

```
fredf1 <- data.frame(id, FRE1)
fredf2 <- data.frame(id2, FRE2)
fredf3 <- data.frame(id3, FRE3)
fredf4 <- data.frame(id4, FRE4)

names(fredf1)[names(fredf1) == 'FRE1'] <- 'FRE'
names(fredf1)[names(fredf1) == 'id'] <- 'pointid'
names(fredf2)[names(fredf2) == 'FRE2'] <- 'FRE'
names(fredf2)[names(fredf2) == 'id2'] <- 'pointid'
names(fredf3)[names(fredf3) == 'FRE3'] <- 'FRE'
names(fredf3)[names(fredf3) == 'id3'] <- 'pointid'
names(fredf4)[names(fredf4) == 'FRE4'] <- 'FRE'
names(fredf4)[names(fredf4) == 'id4'] <- 'pointid'

total <- rbind(fredf1, fredf2, fredf3, fredf4)
write.csv(total, file = "F:\\RxCADRE_L2F_2012\\Total_New_FRE.csv" )
```